NUMERICAL UNDERSTANDING OF μ TAS

A DISSERTATION

*Submitted in partial fulfillment of the
requirements for the award of the degree
of*

MASTER OF TECHNOLOGY

in

MECHANICAL ENGINEERING

(With Specialization in Thermal Engineering)

Submitted by

SUBHAMOY PAL

Enrollment No-15541019

Under the supervision of

Dr. ARUP KUMAR DAS

Department of Mechanical & Industrial Engineering

INDIAN INSTITUTE OF TECHNOLOGY ROORKEE

CANDIDATE'S DECLARATION

I hereby declare that the work carried out in this seminar titled "**Numerical Understanding of μ TAS**" is presented on behalf of partial fulfillment of the requirement for the award of the degree of **Master of Technology** with specialization in **Thermal Engineering** submitted to the department of Mechanical **& Industrial Engineering, Indian Institute of Technology Roorkee, India**, under the supervision and guidance of **Dr. Arup Kumar Das**, Assistant Professor, MIED, IIT Roorkee, India.

I have not submitted the matter embodied in this report for the award of any other degree or diploma.

Date:

Place: **Roorkee**   **(Subhamoy Pal)**

Enrollment no-15541019

CERTIFICATION

.

This is to certify that the above statement made by the candidate is correct to the best of our knowledge and belief.

Dr. Arup Kumar Das

Assistant Professor,
MIED, IIT Roorkee,
UK-247667, India.

ACKNOWLEDGEMENT

I wish to express my deep sense of gratitude and sincere thanks to my guides **Dr. Arup Kumar Das** of Mechanical and Industrial Engineering department, IIT Roorkee, for being helpful and a great source of inspiration. I would like to thank them for providing me with an opportunity to work on this excellent and innovative field of research. Their keen interest and constant encouragement gave me the confidence to complete my work. I wish to thank them for their constant guidance and suggestions without which I could not have successfully completed this dissertation.

I am very thankful to my parents & all of my friends for their never ending encouragement in bringing out this dissertation report.

Date: **Subhamoy pal**

Place: Roorkee   Thermal Engineering

Enrol.No. 15541019

ABSTRACT:

Common feature of µTAS is impact on a droplet on a microfluidic channel for functional analysis. It has been observed that both hydrophilic and hydrophobic nature has their usual applications but shifting of wetting mode is also important for µTAS. One such mode of wetting mode shifted is electrowetting. In the present study droplet impact using electrowetting has been studied numerically.

A coupled electro hydrodynamic model is used to explore the phenomenon of droplet impact on a charged surface. The spatio-temporal electric field is obtained from the solution to Poisson and charge conservation equation. The electrostatic forces are coupled with hydrodynamics by incorporation of Maxwell stress term of the two-phase momentum equation. Geometry of the foot print of the charged region is varied to control the contact line mobility. The electrical stress generated near the three phase contact-line due to the presence of electric field constrains its motion in the desired direction and causes a change of impact behavior. It can be observed that a hydrophilic surface shows hydrophobic characteristics when the droplet is collided with it at a concentric ring shaped charged regions. As the phenomenon is mainly governed by the interplay between electrostatic, capillary and inertia forces it is explored through the parametric variation of applied voltage as well as parametric variation of contact angle and impact height. It has been observed that the application of voltage can change hydrophilic surface into a bouncing hydrophobic one for application of µTAS. The outcome of the present study can be utilized to develop a vast range of engineering surfaces for various applications like drop wise condensation, anti-corrosion and self- cleaning and microfluidics.

CONTENTS

LIST OF FIGURES

LIST OF TABLES

NOMENCLATURE

ρ_e	Charge density
V	Electric potential
ρ_m	Mass density
C_H	Helmholtz capacitance
ϵ_D	Permittivity
ϵ_0	permittivity of air
T_m	Maxwell stress tensor
K	Conductivity
p	pressure
θ	contact angle
$\theta 0$	contact angle without voltage
t	thickness of the dielectrics
u	velocity
T_v	viscous stress tensor
δ_s	direct delta function
κ	mean curvature of interface
q_c	Volumetric charge concentration
e	Volumetric electric force
α	liquid-volume fraction
σ	interfacial energy
σ_{sv}	interface energies (solid-vapour)
σ_{sl}	interface energies (solid-liquid)
σ_{lv}	interface energies (liquid-vapour)
ΔP	Pressure drop
γ	surface tension
V	Voltage
ρ_a	density of gas
ρ_w	Density of water
μ_a	viscosity of gas
μ_w	viscosity of liquid

CHAPTER 1

INTRODUCTION

Droplet wettability is an important parameter which changes the rate of reaction of heat transfer from engineering devices. There are two extremities of wettability namely hydrophilic and hydrophobic.

1.1 Hydrophilic and hydrophobic

The terms "hydrophilic" and "hydrophobic" define the opposite extremities of wettability which are quite common to microfluidics and appeared in the literature for past few decades. Drop manipulation in microfluidics is quite common in biological energy and chemical sectors. Science and engineering involved in mobilization of drop using attraction of substrates characteristics is known as micro total analysis system (µTAS). µTAS uses wettability characteristics of the surface for driving force. Next we describe extremity of the wetting characteristics. A deliquescent surface has robust affinities to water whereas hydrophobic surface repels water. In this band of extreme wettability solid show different wettability characteristics and manipulation of drop contact angle with surface in used for various engineering application. Even it finds application in theoretical phase system of oil-water-air.
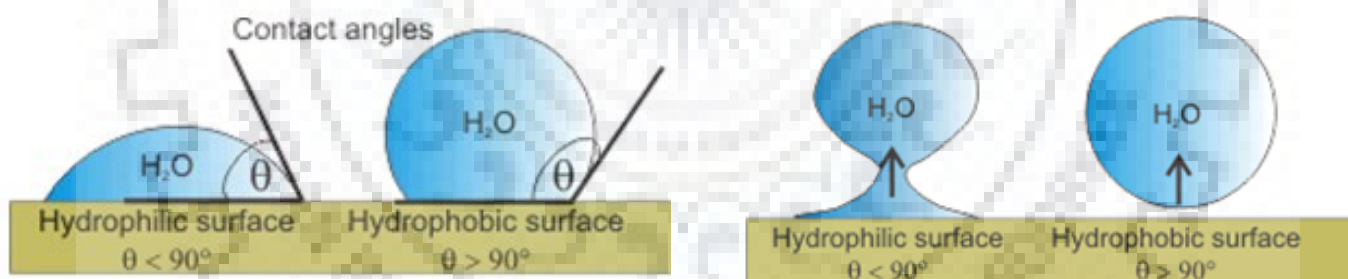
Figure 1.1: Representation of hydrophilic and hydrophobic behavior

The term "hydrophobicity" originates from two ancient Greek words hydro (water) and phobos (fear) and can be well describe from property of substrate molecules. The hydrophobic substrate molecules once come in contact of water gets repelled from it towards the water molecule. Hydrophobic property results from the absence of any permanent or elicited electrical dipole between water and substrate molecule and lack of ability to create chemical element bonds. Therefore, hydrophobic molecules act with water solely through London dispersion force. Completely offsite molecular affinity is observed in case of hydrophilic surface. Surface having

hydrophilic molecules get attracted by water molecules and forms dipole moments frequently. Macroscopically hydrophobic surface exhibit massive contact angle when a water drop is placed at top of it. It had been assumed that on a hydrophobic surface the contact angle has to be 90° or larger. On the other hand hydrophilic surface shows acute contact angle. The behavior and wetting characteristics of each these surfaces square measures delineate in Figure 1.1. At first static drop placed on the surface is shown and next during withdrawal of drop schematic representation of phenomenon is shown.

1.2 Contact angle criterion

Water (or other polar liquids) is preferred on hydrophilic surface in the vicinity of nonpolar phase such as air or oil. It is therefore no surprise, as already mentioned earlier, that 90 degrees of water contact angle measured in the air environment is traditionally a popular criterion between hydrophilic and hydrophobic surfaces. Hydrophobic surface has contact angle is larger than 90° ($\theta > 90^{o}$) and hydrophilic one settles with contact angles of $\theta < 90^{o}$.

1.3 Droplet impact on superhydrophilic and superhydrophobic surfaces

Majority of the µTAS applications depend upon impact of droplet on micro channel for functional degradation of the matrix fluid. Hence, the operation of these devices depends on how water will behave after impact. Matrix fluid sticking on the surface will provide more retention time for contact with chemicals and on the other hand superhydrophobic bouncing will enhance heat and mass transfer by repetitive contact with the hot surface. Hence, it is required to study the droplet impact on these surfaces quite carefully.

Upon impact on superhydrophilic surfaces, drop stretches on that and occupies a lot of contact space as shown in Figure 1.2. It will never leave contact with the surface and increase the area of contact. This behavior is useful for location dependent chemical reactions and heat transfer. One will clearly observe from the figure that at the rim of the drop, under extreme stretch small daughter droplets is being created due to surface tension. Extent of instability increases within flow velocity.

Superhydrophobic surface is special designed substrate which water (advancing) contact angle is a minimum of 150° and the contact angle hysteresis between successive advancing

and retarding case do not exceed 5-10°. Superhydrophobic surfaces are found in one biological specimens, and their artificial substitutes are factory-made by chemical, physical and/or mechanical modifications of surface material. A typical feature of superhydrophobic surfaces is micro level topography, which shows micro or nano-sized asperities/posts. Some hydrophobic surfaces are now prepared by lotus leaves or similar plates.
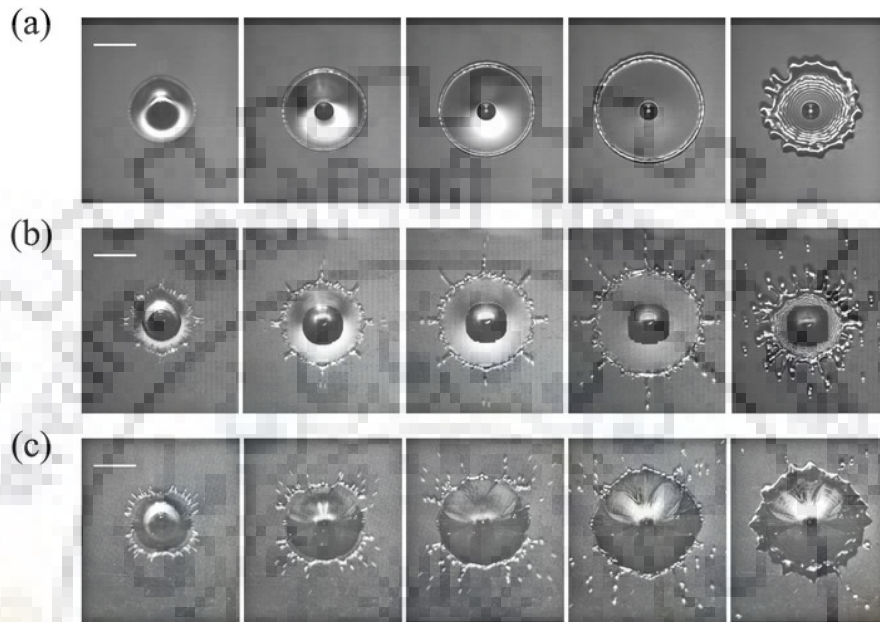
Figure 1.2: Droplet impact on hydrophilic surface by Tsai et al. [1]

Impact of a droplet on hydrophobic surface shows typical time rating wetting phenomena. At the beginning it stretches on the surface but after some time it retracts back and comes out of the surface to jump against gravity. The jumping behavior is shown in Figure 1.3 on hydrophobic surfaces. Essentially it requires contact angle more than 120°.
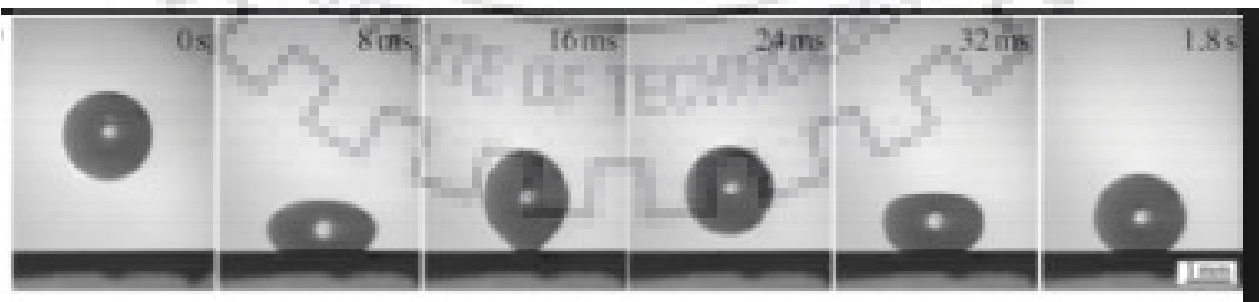
Figure 1.3: Droplet impact on hydrophobic surface by Bhushan et al. [2]

Both hydrophilic and hydrophobic surface are having unique advantage and applications. But in the era of function on demand conversion from hydrophilic surface to hydrophobic or

hydrophobic surface to hydrophilic is very much necessary. It will find application in microfluidic valves, pumps and spray cooling. Conversion of hydrophobic surface to hydrophilic one namely using magnetic field, sound wave, thermal gradient. One of the most important and researchable area is by the application of electric field (Figure 1.4). Target has been made to apply electric field to one hydrophilic surface and convert it to hydrophobic one. Application of electric field in μTAS surfaces is commonly known as electrowetting. In next section, description has been given related to fundamental understanding about chances of droplet wettability by application of electric field.
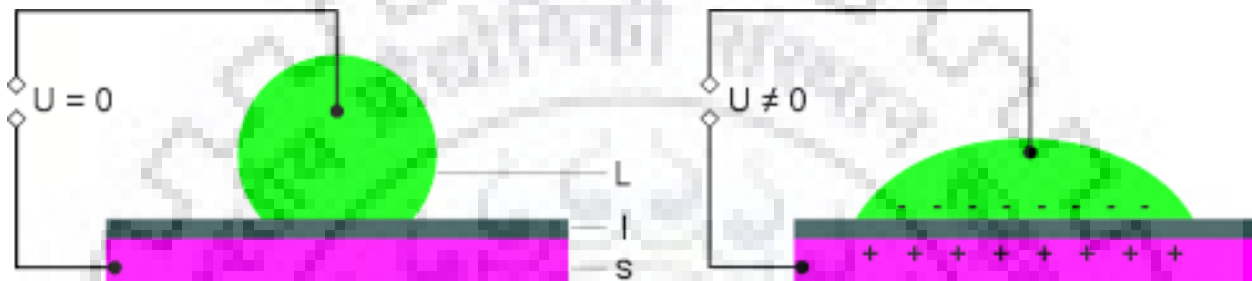
Figure 1.4 Generic idea of wettability shift after application of electric field.

1.4 Electrowetting

Manipulation of wettability by the application of external electric field is referred as electrowetting. The phenomenon of electrowetting first investigated by Lippmann [3] for a conducting liquid indirect contact with metal surface. However it's application was limited due to the possibility of electrolysis of the liquid medium. Berge[4] circumvented this problem by introducing a di-electric layer between the liquid and the solid surface. This technique is known as electrowetting on di-electrics (EWOD). After this modification it is used substantially in various applications of drop manipulation. Electrowetting is advantageous compare to other drop manipulation technique like thermo capillary action, magnetic field, vapor bobble base pumping etc. due to its low cost, high controllability and precession.

The phenomenon of electrowetting can be explained by thermodynamic, energy minimization or by electro-mechanical approaches. According to thermodynamic approach the reduction in interfacial energy between solid and liquid at the application of electric potential, is the reason for increased wettability or decrease in contact angle. Under external electric field when a droplet is kept in touch with a conducting solid, there is a formation of

electric double layer. Considering Gibbs free energy minimization the charge concentration (ρ_e) at the double layer can be expressed as:

$$-\rho_e = \frac{\partial \sigma}{\partial V}\bigg|_{\mu} \qquad (1.1)$$

where σ and V are interfacial energy and electric potential respectively. Considering constant thickness of double layer the specific Helmholtz capacitance (C_H) can be written as:

$$C_H = \frac{\partial \rho_e}{\partial V} \qquad (1.2)$$

Substituting the value of ρ_e (from equation 1.1) to equation 1.2 and integrating, the equation to measure the variation of interfacial energy can be obtained as:

$$\sigma_{sl}(V) = \sigma_{sl}(0) - \frac{C_H}{2}V^2 \qquad (1.3)$$

where $\sigma_{sl}(V)$ and $\sigma_{sl}(0)$ are solid–liquid interfacial energy with and without electric potential respectively. Now once the interfacial energy is obtained at a particular potential, Young's equation ($\sigma \cos\theta = \sigma_{sf} - \sigma_{sl}$)can be considered to calculate the change of contact angle. Thus, the change in contact angle due to electric potential can be expressed as:

$$\cos\theta = \cos\theta_0 + \frac{C_H V^2}{2\sigma} \qquad (1.4)$$

where θ and θ_0 are the contact angle with and without electric field. This equation is known as Young-Lipmann equation. In real implementation of electrowetting in dielectrics, thickness of the insulating layer is much higher than the double layer thickness. Thus, the Helmholtz capacitance (C_H) can be replaced by the capacitance of the dielectric layer. As a result dielectric Young-Lipmann equation takes a form as:

$$\cos\theta = \cos\theta_0 + \frac{\varepsilon_0 \varepsilon_D V^2}{2\sigma t} \qquad (1.5)$$

where ϵ_D and t are the relative permittivity and thickness of dielectric layer. ϵ_0 is the permittivity of air. The above expression of contact angle change can also be obtained from

electro-mechanical and energy minimization approach. Electro-mechanical approach is mentioned details in chapter 4.

1.5 Types of electrowetting on dielectric (EWOD)

Two different types of EWOD-based microsystem have been developed : single plate where the sessile droplet is sitting freely on a horizontal solid substrate and double plate or parallel plate where the droplet is covered between two plate. Schematic of the systems are shown in Figure 1.5. Each of this system has its own advantagees. Drop to dispense , motion,and splitting are easier about covered EWOD system, whereas mixing & evaporation are preferably performed in open configuration. With some hybrid designs, these two types of EWOD are interfaced such that droplet motions between the covered and an open region is possible under electrowetting actuation.
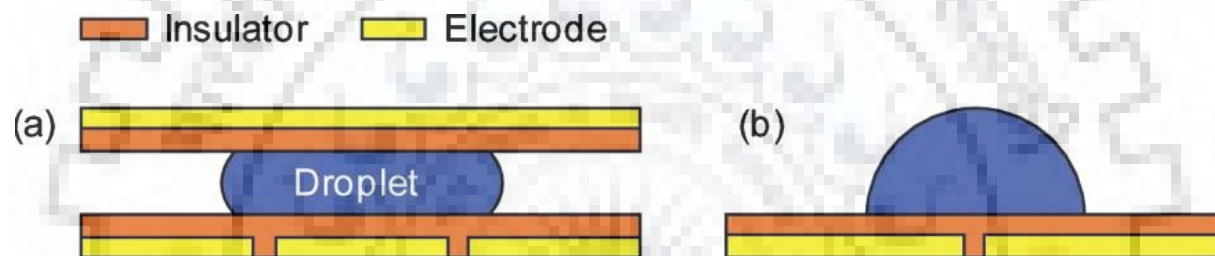
Figure: 1.5 (a) parallel plate EWOD & (b) single plate EWOD

Single plate:

In the single-plate configuration, however, the cover plate is removed, and both actuation and reference voltages are applied to base-plate electrodes. In this case, the droplet is in an electrically floating state, and the electrostatic potential for the droplet is between the actuation voltage and reference voltage. In coplanar electrodes designs, both buried activation electrodes and exposed ground electrodes to maintain the droplet grounded are located on the base plate of multiple conducting layers.

Parallel plate:

The parallel-plate configuration has a base plate patterned with an array of discrete electrodes and a cover plate in a parallel configuration. Droplets are sandwiched between the two plates, normally surrounded by a nonpolar liquid such as silicone oil to prevent evaporation and to reduce the contact angle hysteresis. A reference voltage is applied to the cover-plate electrode, and successive transport of a droplet is induced by sequentially applying electrical signals to base-plate electrodes just beneath or nearby the droplet.

1.6 Application of micro total analysis system (μTAs)

μTAS is a multidisciplinary field in engineering, physics, chemistry, biochemistry, nanotechnology, and biotechnology, with practical applications to the design of systems in which low volumes of fluids are processed to achieve multiplexing, automation, and high-throughput screening. Electrowetting is the most efficient technique to control small volume of liquid. In general, one can use electro-wetting as a tool to manipulate the wetting properties in the cases where a droplet is situated over a solid surface or confined to the solid walls of various applications. Some specific application are mentioned bellow.

1.6.1 Lab on a chip

A lab-on-a-chip (LOC) is a device (Figure 1.6) that integrates one or several laboratory functions of a single chip of only millimeters to a few square centimeters to achieve automation and high-throughput screening. LOCs deal with the handling of extremely small fluid volumes down to less than pico liters. Lab-on-a-chip devices are a subset of Micro-electro-mechanical systems (MEMS) devices and often indicated by "Micro Total Analysis Systems" (μTAS) as well. Electrowetting has many successful implementation inside lab on chip devices for translation, agglomeration and bifurcation of these small liquid volume.
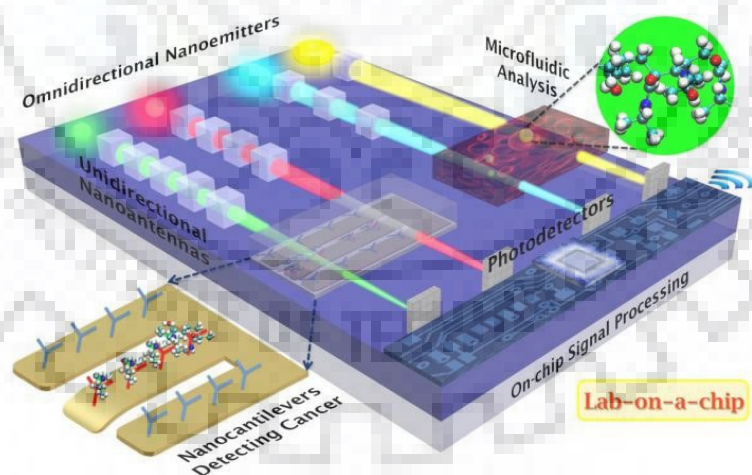
Figure: 1.6 Lab-on-a-chip.

1.6.2 Lenses with continuous variable focal length

Electrowetting has also successfully used to create liquid lenses with continuous variable focal length. Figure 1.7 shows a typical design of electrowetting lenses developed by Kuiper [5] research group. Here two immiscible liquid confined in a close chamber. Arrangement has been made to exact electric potential across the conducting liquid. Changing contact angle with the increasing electric potential result in a continuous variation meniscus curvature and thus in focal length.
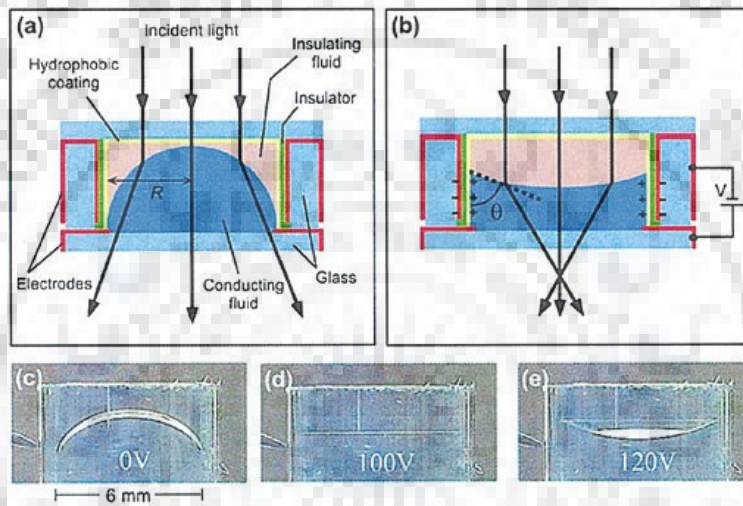
Figure:1.7 Design of electro wetting lenses devolved by Kuiper et al. [5].

1.6.3 Display technology

Electrowetting has also been used in electronic displays like e-reader, mobile phone and MP3 player screen etc. A typical design of electrowetting has presented in figure 1.8 . Each pixel of a electrowetting display confines oil dissolved dye along with a conducting liquid. Initially the oil spades over the whole pixel floor. This configuration reflex very less amount of incident light and thus the pixel appears as a dark spot. With an application of an electric field the adopted contact angle push the oil layer aside; exposing the bottom surface of the pixel. This results in lays absorption of light rays. With proper control of electric potential simultaneously at an array of pixel can render a desire image
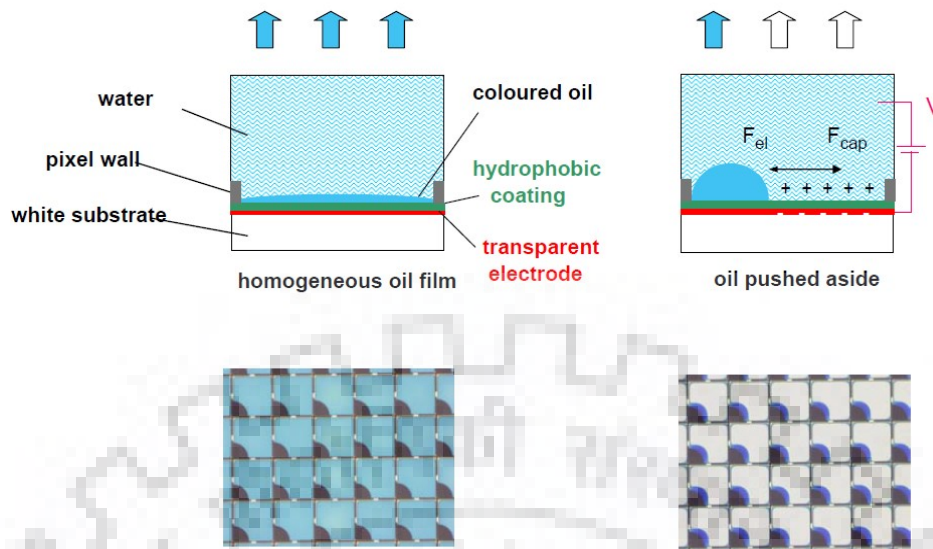
Figure 1.8: design of electrowetting based display by Zichuan et al. [6]

1.6.4 <u>Aduptive chip cooling</u>

Over the last few decades there is a substential groth of high energy density semiconducter devices in various elctronic industry. During the oparation of devices removal of heat is essencial in order to minimise thermal stresses. Electrowetting has been successfully implimented in such applications. Due to the ease of control, an electrical actuation system can provide an on demand droplet supply to a specific location of high heat genaration. Thus the proper control arrangement a electrowetting system can be used as a aduptive thermal manegement system in various semiconducting devices.

CHAPTER 2

LITERATURE SURVEY

After the first observation by Lipmann[3] and modification by Burge [4], a substantial amount of research has been performed to analyse the feasibility of electrowetting in various fields of engineering, biochemistry and clinical diagnosis. Numerous experimental endeavours has been spent to use electrowetting as a technique for droplet manipulation like translation, agglomeration, splitting or bifurcation and dispensing inside lab-on-a-chip or μ–TAS devices.

Cho et al. [7] successfully actuated droplets over a electrowetting on a dielectric system. They also provided design criteria for the bifurcation of a droplet over a solid surface.

Cho et al. [8] actuated droplet only at 18 V. However the actuation was reputable and consistent at 25 V. They achieved a drop velocity of 250 mm/s over a Teflon and oxide layers coated surface with actuation potential of 150 V.

Eow et al. [9] experimentally investigated drop deformation and break up under a field strength between $3.5X10^5$ and $3.8X10^5$ V/m. It was observed that there exit a critical field required for drop deformation depends on droplet size.

Hong et al. [10] used electro wetting technique to transfer a droplet on an overhead plane by inducing a vertical electric field. However the requirement of electric field was high. They also provided the possible electrode design to reduce the required actuation potential.

Aminfar and Mohammad pourfard [11] used lattice Boltzmann method to investigate droplet agglomeration. They also analysed the stability of a droplet in its vapour.

Arzpeyma et al. [12] numerically investigated droplet translation by a coupled electro hydro dynamic model based on volume of fluid formulation. However the coupling is performed through Young Lipmann equation; Maxwell stress produced due to the electric field was not consider in the momentum equation.

Datta et al. [13] performed numerical simulation by following pure electro mechanical approach to understand the dynamics of uphill droplet movement. They coupled the electric

phenomenon with hydrodynamics by incorporating the volumetric electric force in the transient Navier stoke equation. They also produced a voltage map to obtain the threshold voltage required for droplet up climbing.

Banerjee et al. [14] successfully translated a sessile droplet over an array of electrodes. The analyzed the effect of electric permittivity and thickness of the dielectric layers on electro wetting performance. They concluded that the electric permittivity have higher influence than the thickness of the dielectric layer.

Dutta et al. [15] performed analytical investigation to analyses effect of wetting nature of the surface on electrostatic droplet actuation along an incline plane. They also produce a voltage map required to a steady constant velocity of drop motion along a curve liner path.

Lee et al. [16] experimentally investigated the impact dynamics of a droplet on an electrically actuated surface. They provide a alternatively a stretched and upstretched Teflon layer to insulate the droplet form the bare metal surface. They reported that the response of upstretched Teflon layer was less than stretched one.

Daub et al. [17] performed molecular dynamic study to analyzed influence of electric field on droplet splitting over a solid surface. They reported that, in presence of parallel electric field, liquid spreads asymmetrically on solid surface. Moreover, the leading and trailing contact angles are different.

Ghazian et al. [18] numerically investigated droplet oscillation under AC electric potential. They reported that, there exists a critical resonance frequency, at which the droplet interface starts vibrating vigorously. It was observed that the resonance frequency strongly depends on contact angle and surface properties.

Kuo et al. [19] experimentally proved that droplet actuation could be much faster inside an oil medium rather than gaseous phase. They also provide a hydro dynamic model to analyzed the mechanism of droplet movement inside the oil medium.

Wang et al. [20] performed numerical simulations by dissipative particle dynamic method to comprehend droplet impact on solid surface. They reported that the dynamic properties of droplet like bouncing, pinning, contact line motion depends on material wettability, the fraction of pillars in the structured surface and the impact velocity of the droplet.

Vallet et al. [21] investigated the threshold condition of electrostatic wettability manipulation. They observed that when a droplet of non-conducting medium is subjected to electric field, an instability generated near the contact line, which ejects small daughter droplets in the outward direction. They reduced the instability by use of salt solution, however it shows a state of saturation beyond a certain electric potential. Their investigation reveals that the ionization of air at the vicinity of contact line is the cause of the saturation.

Bhadhur and Garimella [22] provides an analytical model to investigate transition of wetting state under external electric field. Based on energy minimization frame work they estimated the electrically manipulated contact angle on rough surfaces.

Song et al. [23] carried out molecular dynamic simulation to analise spreading of a nanosize water droplet over a silicon substrate. Their study reviles that in a electric field parallel to the solid surface droplet can take a asymmetric shape. This asymmetry can increase with the augmentation of electric field. However at high electric field, the wetting front dimineses this asymmetry in the leading and trailing front.

Yuan and Zhao [24] performed to characterized the propagation of spreading front under external electric field. Their study reviles that electrostatic droplet spreading follows power law. The coefficient and exponent of the power law depends on a magnitude of the applied potential.

Motivation of present work:

Complex dynamics of electrowetting is studied in numerous endeavors. Majority of these investigations are discussing about electrostatic drop manipulation over solid surfaces,

whereas very few have tried to explore the electrostatic actuation to control drop impact on a surface. The geometry of the foot print of the charged region can be varied to control the contact line mobility. The electrical stress near the three phase contact-line due to the presence of electric field can constrains its motion in the desired direction causing a significant change in the impact behavior. Thus, in the present study, electro-hydrodynamic simulations have been performed to investigate the phenomenon of drop impact on a concentric ring shaped electrode array.

CHAPTER 3

GAPS IN LITERATURE

Based on the literature review presented in previous chapter, I found the following gaps in the literature:

- ➢ A thorough analysis describing behavior of water droplet on hydrophilic and hydrophobic surface is due for the application of electric field.

- ➢ By the application of electric field over the surface one hydrophilic surface can convert to hydrophobic surface or vice versa by applying the negative voltage.

- ➢ Basic reason for droplet wetting mode shifting based on electric field has never targeted in literature.

- ➢ No study has been reported on the effect of voltage, effect of impact height, as well as effect of hydrophobicity with time domains for impact on droplet over the surface.

- ➢ Effect of negative electric field over the hydrophilic or hydrophobic surface is also due in this electric field.

- ➢ Tuning of a surface between hydrophilic to hydrophobic by the help of electric field is also a gap between literature.

- ➢ Superhydrophobic behavior of water droplet upon impact is never tried on engineering surfaces using electric field.

After pointing out the gaps in literature, I framed the following objectives for my research:

- • Propose, new technique for shifting of wetting mode by application of electric field.
- • Convert hydrophilic surface to a hydrophobic one by application of voltage in substrates.
- • Using numerical simulation proved the concept of shifting in wetting mode.
- • Obtain fluidic reasons for shifting of wetting mode.
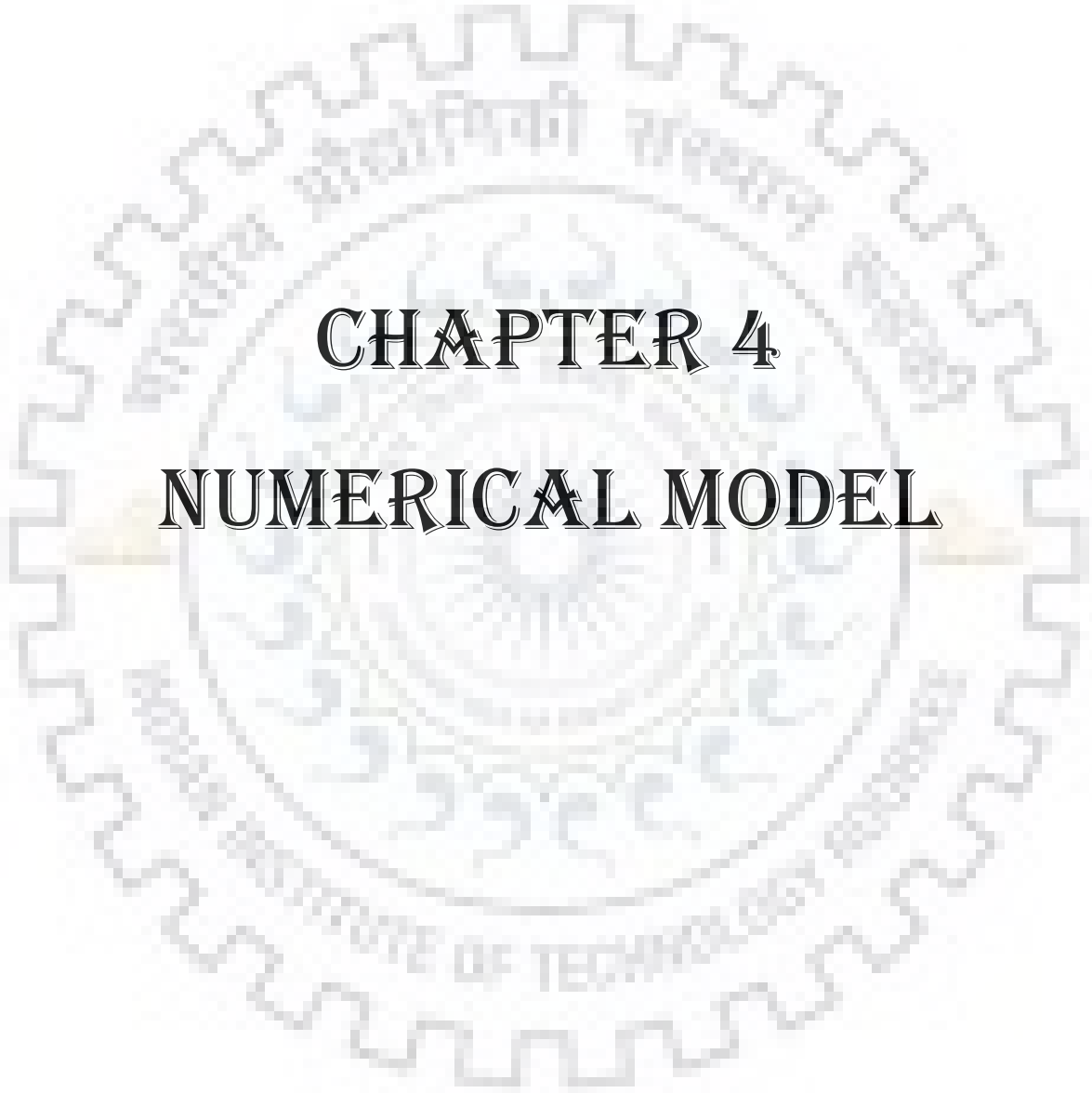
CHAPTER 4

NUMERICAL MODEL

In this chapter we describe the governing equations and model development for numerical simulations.

4.1 <u>Governing equations</u>

An electro hydrodynamic phenomenon occurs when a liquid is exposed to an external electric field. Electrowetting is archetypal example of an occurrence of this kind. In this technique a small volume of liquid (in form of a droplet) is subjected to AC or DC electric potential. Due to the electrostatic the free ions and the dipoles present in the liquid reorganize themselves in accordance with the applied field. This results in the accumulation of charge near the interface regions. The sharp curvature in the wedge shaped contact line vicinity causes a high charge concentration build up in this region. Thus, the electric field produces higher stress near the contact line. The electrostatic force imparted on this region is schematically shown in Figure 4.1. The vertical component of this electrostatic force is balanced the by the stress generated at the solid surface. However, the horizontal components try to drag the interface outward. This reduces the apparent contact angle, keeping the equilibrium one unaltered. The force density due to the electric field can be expressed by

$$F_e = \rho_e E - \frac{1}{2} E^2 \nabla \varepsilon \qquad (4.1)$$

From the momentum conservation principal this force can also be estimated from the integration of momentum flux density over the confining surface:

$$(F_e) = \int (T_e).ndA \qquad (4.2)$$

where n is unit normal of confining surface and T_e is the Maxwell tress tensor:

$$T_e = \varepsilon(EE - \frac{E^2}{2}I) \qquad (4.3)$$

Simulation of electro-hydrodynamic can be done by introducing the electric force (shown in equation 4.2) as a source term in the momentum equation. Thus, coupled electro hydrodynamic mass and momentum conservation equation can be written as:

$$\nabla.u = 0 \tag{4.4}$$

$$\rho(\frac{\partial u}{\partial t} + u.\nabla u) = -\nabla p + \nabla.T_v + F_e + \sigma\kappa\delta_s n \tag{4.5}$$

where u and p are velocity and pressure, T_v is viscous tress tensor. δ_s is direct delta function which enables the surface tension (σ) force to act at only at the interface, κ is the mean curvature of interface. In a typical electro-hydrodynamic system the electrostatic stress deforms the interfaces dynamically. This in turn alters the charge and potential distribution inside the flow domain. The spatial variation potential and charge can be obtained by solving Poisson equation and a charge conservation equation:

$$\nabla.(\varepsilon\nabla\phi) = -\rho_e \tag{4.6}$$

$$\frac{\partial\rho_e}{\partial t} + \nabla.(\rho_e u) = -\frac{K}{\varepsilon}\rho_e \tag{4.7}$$

Once the spatial variation of charge electric field is calculated from above equations, the electric force can be computed by:

$$F_e = \nabla.T_e \tag{4.8}$$
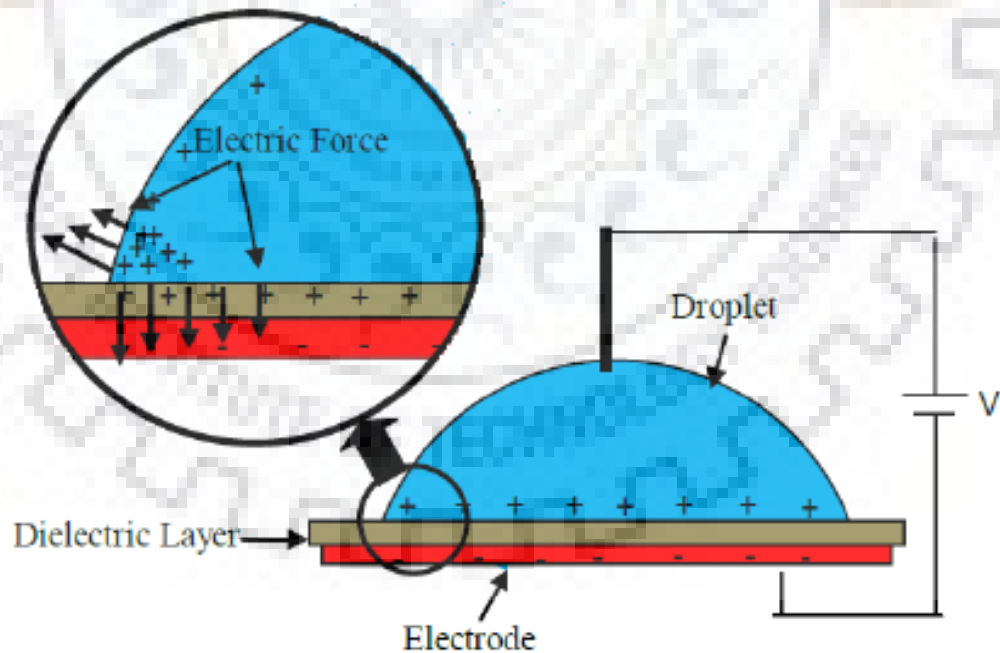
Figure 4.1: Schematic representation of charge and electrostatic force distribution near contact line.

In the present study, the technique of electrowetting is adopted to manipulate a droplet after impact on a solid surface. The physical configuration of the present setup is depicted in Figure 4.2. To control the motion of the contact line, concentric ring shaped electrodes are considered. Electric potential is applied to the alternative electrodes (red rings in Figure 4.2). The electrodes between the actuated ones are kept grounded (blue rings in Figure 4.2). The droplet is allowed to impact at the center of the electrode array. The phenomenon is considered to be axisymmetric.
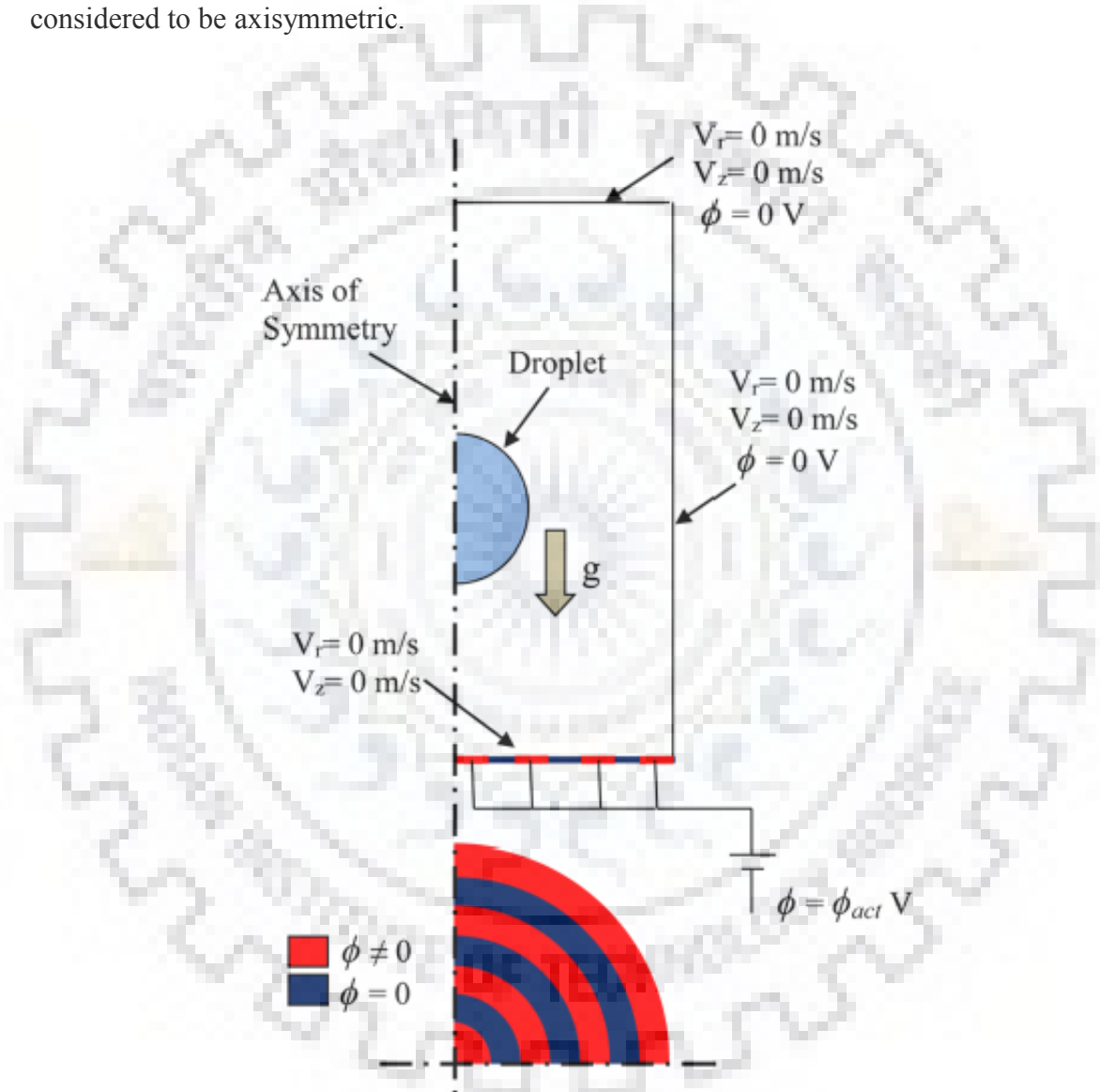
Figure:4.2 schematic representation of the computational domain and electrode arrangement.

4.2 Numerical scheme

Gerris flow solver [25-27] is used to investigate the impact dynamics of the droplet. Gerris is equipped with a electro-hydrodynamic module, where two phase transient Navier stokes

equations are coupled with the electric phenomenon by incorporation of volumetric electric force in a momentum equation. Gerris utilises a finite volume scheme to solve the incompressible conservation equations. The interface in the two phase flow domain is tracked by a piecewise linear volume of fluid (VOF) scheme. It employ a height function formulation to calculate the local curvature. In Gerris, the interface tracking is performed on the basis of liquid volume fraction. The conservation equation for liquid volume fraction can be written as:

$$\frac{\partial c}{\partial t} + \nabla.(cu) = 0 \tag{4.9}$$

where c is the liquid volume fraction. The constitutive equation to obtain density and viscosity can be written as:

$$\rho = c\rho_l + (1-c)\rho_g \tag{4.10}$$

$$\mu = c\mu_l + (1-c)\mu_g \tag{4.11}$$

where ρ and μ are the density and viscosity of the medium. The subscripts l and g signifies liquid and gas phases respectively. Likewise, electric conductivity and permittivity can be derived in the two phase system as:

$$\varepsilon = c\varepsilon_l + (1-c)\varepsilon_g \tag{4.12}$$

$$K = cK_l + (1-c)K_g \tag{4.13}$$

where ϵ and K are the permittivity and conductivity of the medium.

Gerris utilises an quartree/octree adaptive mesh refinement scheme to discretise the domain spatially. The adaptation of mesh refinement is performed on the basis of specified criteria. During adaptation the mesh is refined hierarchically from a root cell (cell of maximum size) to a lowest cell size (leaf cell). In each step in quartree refinement the parent cell is divided into four equal daughter cells (in octree the number of daughter cell in the next immediate step is eight). Thus at n^{th} level of refinement the size of cell will be $\frac{1}{2^n}$ times of the root cell (cell of maximum size).Figure 4.3 elucidates the schematic representation of hierarchical quartree mesh refinement.
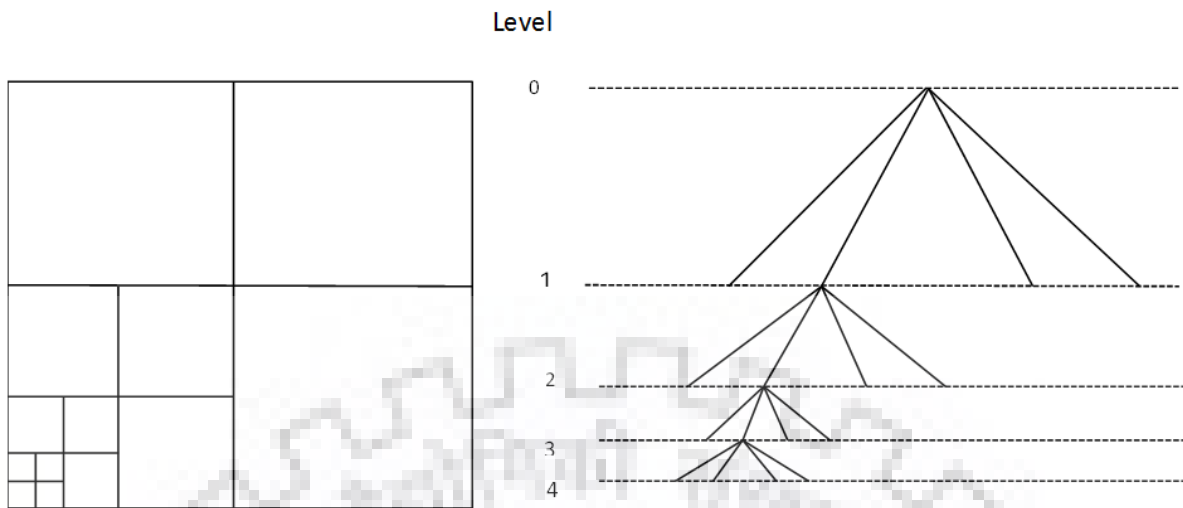
Level

Figure 4.3: Schematic representation of octree special discretization.

Gerris performs controlled access to each level of cell refinement by Khokhlov's [28] fully threaded tree structure. All the cell averaged value of the primitive variables are stored at the centre of each cell. In the present study this is done based on interface location and vortices inside the flow domain. Figure 4.4 shows the distribution of cell inside the flow domain at particular time instants.

(a)   (b)
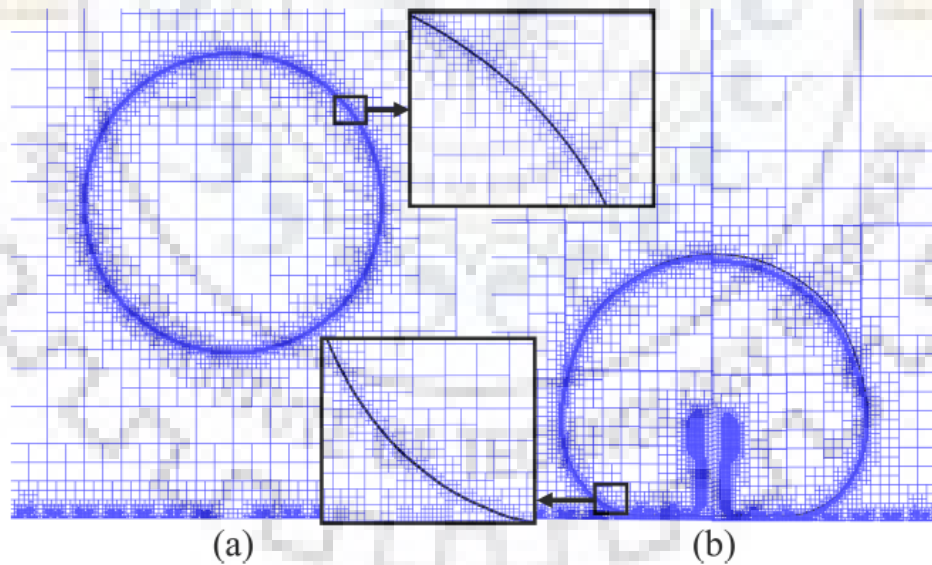
Figure 4.4: Distribution of cells inside of the computational domain

In Gerris, the volume fraction and the pressure are discretized in a second order accurate staggered-in-time scheme. Also, a second order accurate Crank−Nicolson type discretization is employed for the viscous term. Restructuring of the discretized momentum

equation in a Helmholtz type equation enables Gerris to solve it by a multilevel Poisson solver. Gerris employs a time splitting projection method for the discretization of time domain as:

$$\frac{c_{n+\frac{1}{2}} - c_{n-\frac{1}{2}}}{\Delta t} + \nabla \cdot (c_n u_n) = 0 \tag{4.14}$$

$$\frac{(\rho_e)_{n+\frac{1}{2}} - (\rho_e)_{n-\frac{1}{2}}}{\Delta t} + \nabla \cdot [(\rho_e)_n u_n + K_{n-\frac{1}{2}} E_{n-\frac{1}{2}}] = 0 \tag{4.15}$$

$$\nabla \cdot [\nabla(\varepsilon_{n+1/2} \phi_{n+1/2})] = -(\rho_e)_{n+1/2} \tag{4.16}$$

$$\rho_{n+\frac{1}{2}}(\frac{u_* - u_n}{\Delta t} + u_{n+\frac{1}{2}} \cdot \nabla u_{n+\frac{1}{2}}) = \nabla \cdot (\mu_{n+\frac{1}{2}}(D_n + D_*)) + (\sigma \kappa \delta_s n)_{n+\frac{1}{2}} + (F_e)_{n+\frac{1}{2}} \tag{4.17}$$

$$u_{n+1} = u_* - \frac{\Delta t}{\rho_{n+\frac{1}{2}}} \cdot \nabla p_{n+\frac{1}{2}} \tag{4.18}$$

$$\nabla u_{n+1} = 0 \tag{4.19}$$

The above equations the subscript $*$ is used to denote an intermediate provisional value. Taking divergence of equation 4.18 and substituting the value of equation 4.19 results in a Poisson equation as follows:

$$\nabla \cdot (\frac{\Delta t}{\rho_{n+\frac{1}{2}}} \nabla p_{n+\frac{1}{2}}) = \nabla \cdot u_* \tag{4.20}$$

Thus the momentum equation can recasted as:

$$\frac{\rho_{n+\frac{1}{2}}}{\Delta t} u_* - \nabla \cdot (\mu_{n+\frac{1}{2}} D_*) = \nabla \cdot (\mu_{n+\frac{1}{2}} D_*) + (\sigma \kappa \delta_s n)_{n+\frac{1}{2}} + (F_e)_{n+\frac{1}{2}} + \rho_{n+\frac{1}{2}}[\frac{u_n}{\delta t} - u_{n+\frac{1}{2}} \cdot \nabla u_{n+\frac{1}{2}}] \tag{4.21}$$

A multilevel Poisson solver is used to solve the governing equation in a V-cycle. The electric force term is discretized as:

$$(F_e)_{n+\frac{1}{2}} = (\rho_e)_{n+\frac{1}{2}} E_{n+\frac{1}{2}} - \frac{1}{2}(E^2)_{n+\frac{1}{2}} \nabla \varepsilon_{n+\frac{1}{2}} \tag{4.22}$$

Using the framework, numerical simulations are performed for drop impact on a solid ssurface in presence of electric field.

34

CHAPTER 5

RESULTS & DISCUSSION

In this chapter results of numerical simulations are discussed for understanding the fluid dynamics around impacting droplet on a surface under the influence of electric field.

5.1 Parametric variation for understanding drop impact

The principle of electrowetting is applied to control the impact of a droplet on a solid surface. Here, variations on three basic parameters, like voltage, surface hydrophobicity and impact height are tried. Ranges of variations are mentioned below:

5.1.1 Range of voltage:

Influence of voltage of the surface on the droplet impact on electrostatic actuation is tested numerically. A range of voltages from 80 to 120 has been used for simulations. In all the cases the elevation and the contact angles are kept constant at 0.00245m and 90^0 respectively. Following table describes the numerical parameters for different cases.

Table 5.1: Parameters used for understanding variation of voltage

Volt (V)	Contact Angle (θ)	Impact height (m)	Diameter of droplet (mm)	Thickness of electrode (mm)
80	90	0.00245	1	0.1
100	90	0.00245	1	0.1
120	90	0.00245	1	0.1

Table 5.2: Parametric variation of contact angle

Volt (V)	CA (θ)	Impact height (m)	Diameter of droplet (mm)	Thickness of electrode (mm)
100	30	0.00245	1	0.1
100	45	0.00245	1	0.1
100	60	0.00245	1	0.1

5.1.2 Range of surface hydrophobicity:

Effect of hydrophobicity of the surface on the droplet impact under electrostatic actuation has also been tested numerically. The nature of the surface is characterized by the contact angle. A range of hydrophobicity from 30˚ to 60˚ has been tested for this purpose. In all the

cases, the elevation and the actuation potential is kept constant at 0.00245 m and 100 V, respectively. Table 5.2 depicts the numerical parameters for the simulations.

5.1.3 Range of impact height:

Influence of the initial height of the droplet on impact behavior under electrostatic actuation has also been analyzed. Comparisons are made between the droplet contours for three different impact heights, applied to the ring electrodes. Following heights (Table 5.3) are tested to understand the physics behind the droplet jumping. In all the cases, the contact angle and the actuation potential is kept constant at 90^0 and 100 V, respectively.

Table 5.3: Parametric variation of impact height

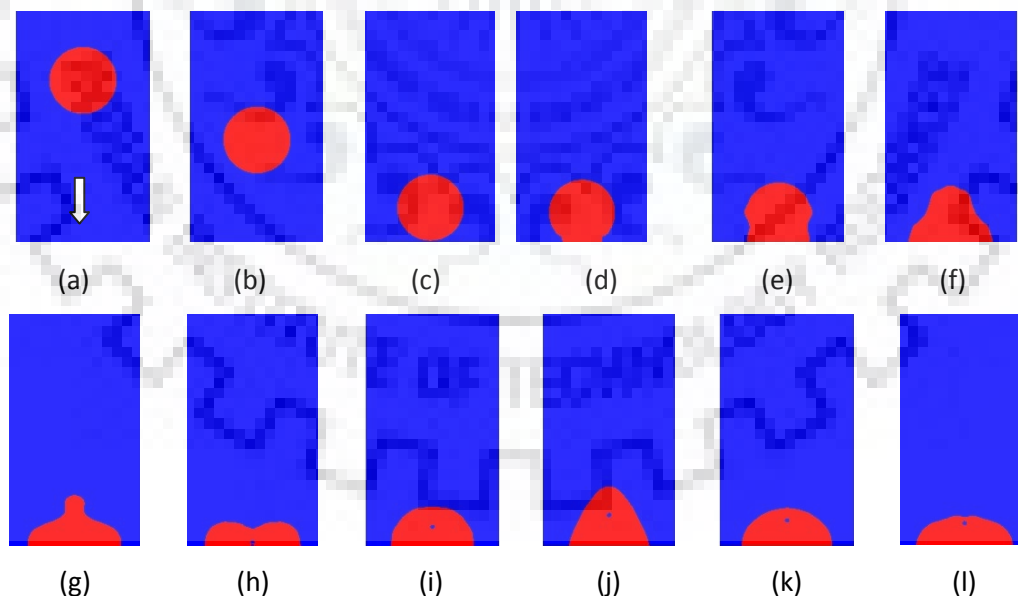| Volt (V)	CA (θ)	Impact height (mm)	Diameter of droplet (mm)	Thickness of electrode (mm)
100	90	1	1	0.1
100	90	1.5	1	0.1
100	90	3.5	1	0.1

Figure 5.1: Phase contour of the droplet during impact with 80 V actuation potential at different time instants. (a) t= 0.0 s, (b) t= 0.0137 s, (c) t= 0.0199 s, (d) t= 0.0203 s, (e) t= 0.0205 s, (f) t= 0.0212 s, (g) t= 0.0217 s, (h) t= 0.0222 s, (i) t= 0.0240 s, (j) t=0.02329 s, (k) t= 0.0254 s, (l) t= 0.0260 s
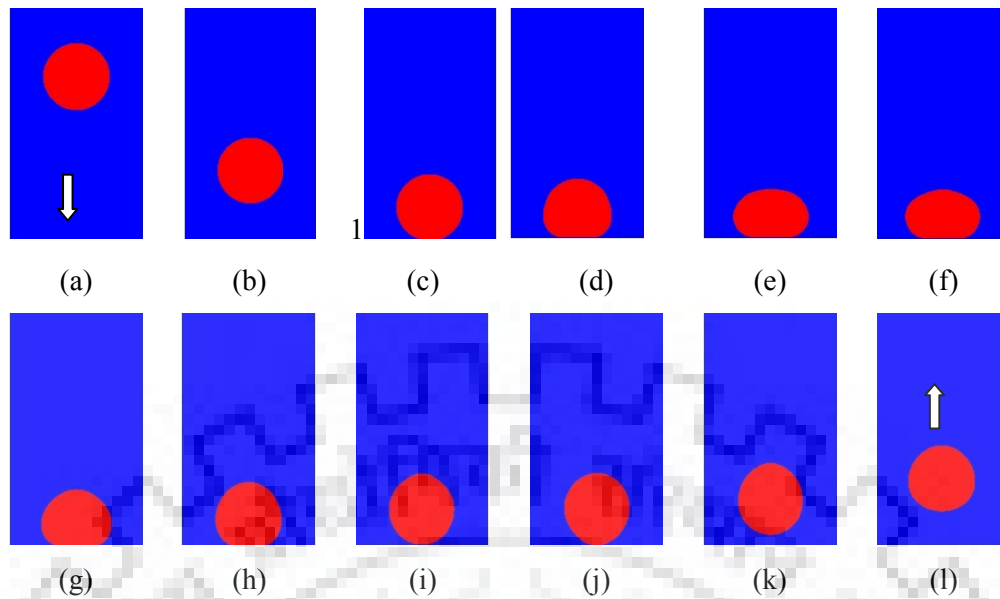
Figure 5.2: Phase contour of the droplet during impact with 100 V actuation at different time instants. (a) t= 0.0 s, (b) t= 0.017 s, (c) t= 0.020 s, (d) t= 0.0207 s, (e) t= 0.0213 s, (f) t= 0.0217 s, (g) t= 0.0222 s, (h) t= 0.0227 s, (i) t= 0.0231 s, (j) t= 0.0233 s, (k) t= 0.0234 s, (l) t= 0.0260 s

5.2 Effect of applied electric field on drop impact

In the present study the droplet is considered to be composed of deionized water. Air is assumed as the surrounding medium. The hydraulic diameter of the droplet is kept constant at 1 mm in all the cases. The width of the ring shaped electrodes is considered as 0.1 mm. Figure 5.1 and 5.2 represent the phase contour of the system at different time instants during the impact for 80 V and 100 V of actuation at the rings, respectively. The equilibrium contact angle is assumed as 90° in both the cases. The droplet sticks to the surface for the case of low actuation potential. The droplet initiates its motion from an elevation of 0.00245 m (Fig.5.1 (a)) and touches the solid surface at t = 0.0199 s (Fig.5.1(c)). Due to the presence the solid surface, the fluid gets restriction in the downward direction and tries to flow in the transverse path. As a consequence the contact line starts spreading (Fig. 5.1(c)-(h)). The kinetic energy of the bulk transformed into the potential energy at the distorted surface. After certain extent stored energy pushes the liquid back and causing an elongation in the longitudinal direction (Fig. 5.1 (j)). Same cycles repeated until the execs energy gets dissipated by viscosity. Thus, the droplet takes a hemispherical shape (not shown in the figure) after showing some initial oscillation. The scenario is different for the impact on surface having 100 V actuation. In this case, initially, the contact line starts to spread over

the surface after the first contact (Fig. 5.2(c)-(e)), however it seizes its motion after a certain displacement along the transverse direction. Thus, the lateral elongation of the droplet is more above the contact region (Fig.5.2 (f)). The stored energy in the elongated droplets drives the liquid in the upward direction. Eventually the droplet gets detached from the surface and moves in the upward direction (Fig. 5.2 (i)-(l)).

To dig down further, we have analyzed the electrical field close to the solid surface. Figure 5.3 shows electrical field contour within the domain at 100 V actuation. From the figure it may be discovered that electric charge is stored inside the droplet. However, the magnitude of the electrical potential remains significant only near the solid surface. This causes an extra force across the contact line and helps the drop to withdraw back by applying retraction force. An understanding of electric field vectors close to the solid surface (shown at the inset of the Figure 5.3) reveals that inside the drop an inward push can be observed due to high concentration of electric charge. An alternating electric field can be observed inside the droplet which stops the drop to spread and retract in the inward direction. At the end it gets bounced back from the surface and shown hydrophobic nature.
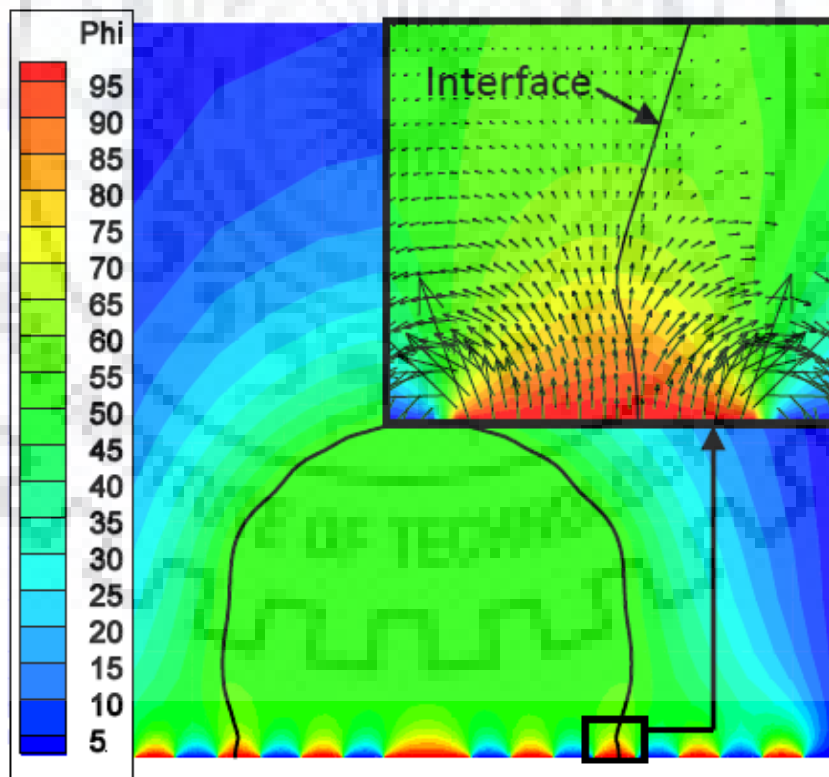

Figure 5.3: Electric field distribution inside the computational domain; actuation potential 100 V
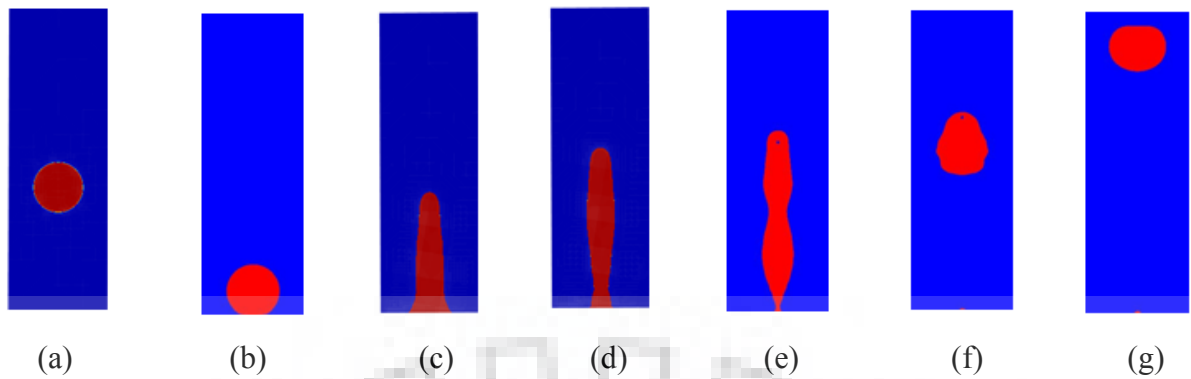
| (a) | (b) | (c) | (d) | (e) | (f) | (g) |

Figure 5.4: Phase contour of the droplet during impact with 120 V actuation at different time instants. (a) t = 0.0 s, (b) t = 0.0206 s, (c) t = 0.0222 s, (d) t = 0.0247 s, (e) t = 0.0268 s, (f) t = 0.03044 s, (g) t = 0.03776 s

As the phenomenon mentioned in the foregoing section mainly occurs due to the electric force, it is interesting to observe the effect of electric potential for it. We have compared the droplet contour for three different voltages applied to the ring electrodes as described in Figure 4.4. Droplet dynamics at applied electric field of 120 V is shown in Figure 5.4. It can be observed that droplet bounces back at a faster rate when applied electric field increases. This can be explained from the increase in extent of applied electromotive force which is a driving force for droplet retractions and hence bounce back. If one makes the comparison of droplet wettability upon application of different electric field, the transition is found in between 80 and 100V.

5.2.1 Variation of Location of the Mass Center

Figure 5.5 also depicts the change in height of the mass center of the droplet as a function of time for different electric potentials. In all the cases the initial height of the droplet is 0.00195 m. Thus, the displacement before the impact is same for all. During the downfall of the droplet voltage has no effect and hence all the curves in Figure 5.5 merge. However, at the electric potential of 80 V, the electrostatic force in not enough to pin down the contact line during spreading in the outward direction. As a consequence, the contact line overcomes the opposing forces at the electrode and the droplet sticks to the surface showing some initial oscillation. On the other hand, for 100 V and 120 V actuation, the electrostatic force suffices to restrict the contact line motion and the droplet rebound in the vertical

direction. Due to the larger electrostatic force for the case of 120 V, it restrains the contact line earlier than 100 V actuation.
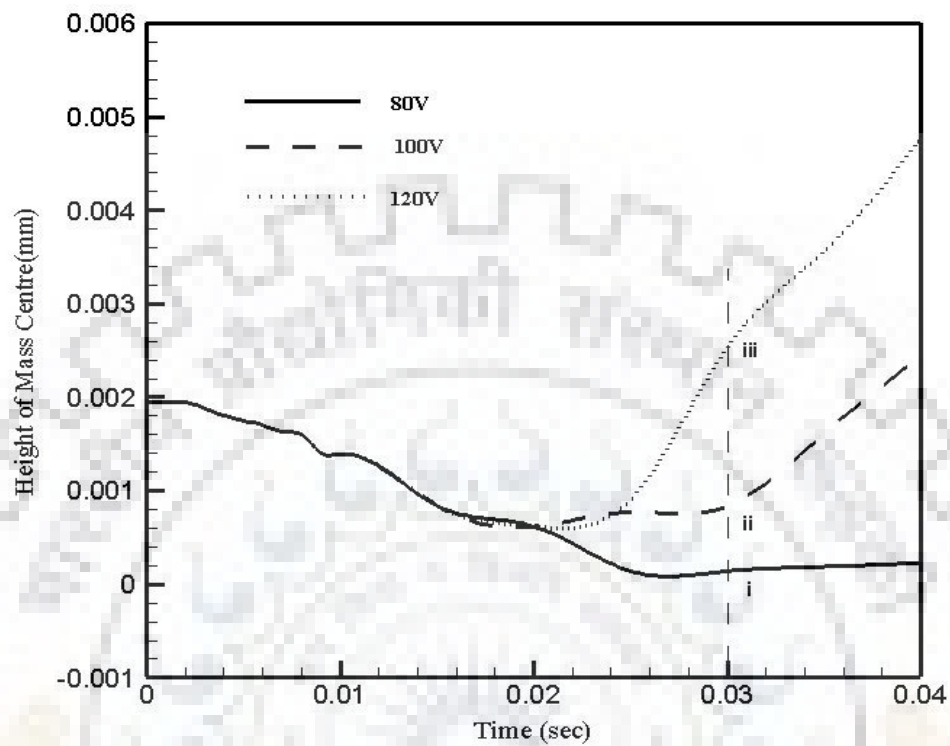

Figure 5.5 Variation of location of the mass center of the droplet as a function of time for different actuation potential; elevation of the drop= 0.00245 m.
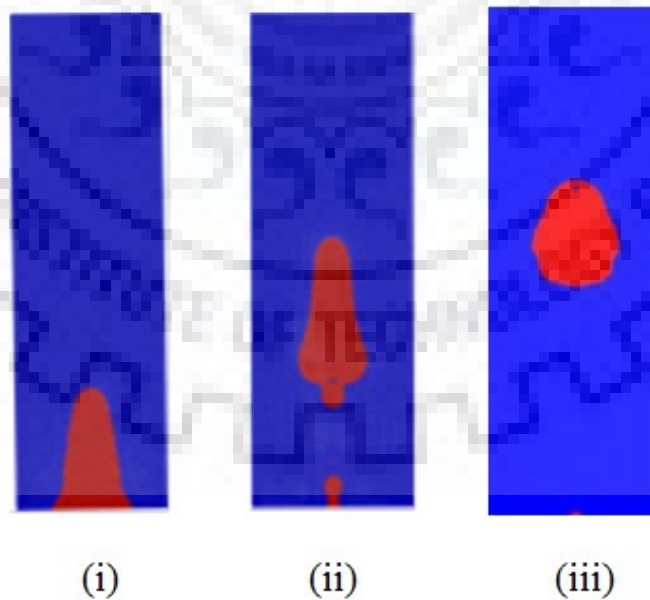

Figure 5.6 Phase contour of the droplet during different actuation voltage at time = 0.03sec; (i) 80 V,(ii) 100 V, (iii)120 V

From Figure 5.6 one can also compare the phase contours of the droplet during different actuation voltages (80, 100 and 120 V) at time 0.3sec. At 80 V the droplet is stuck to the surface till at 0.3 s. But at 100 V droplet is detached from the surface with formation of tiny droplet at the surface. On the other hand, at 120 V, droplet is detached from the surface well before than the 100 V.

From Figure 5.7, one can compare the velocity vectors inside the droplet at three different actuation potential at a same time. When the droplet is retracting back a strong jet is generated through the center of the droplet. Due to this upward jet formation, an upward force is exerted over the droplet and it tries to bounce back or detach from the surface. The jet formation is more predominant when the electrostatic force is more than the surface tension effects i.e. for 100 V as well as 120 V.

100V   80V   120V
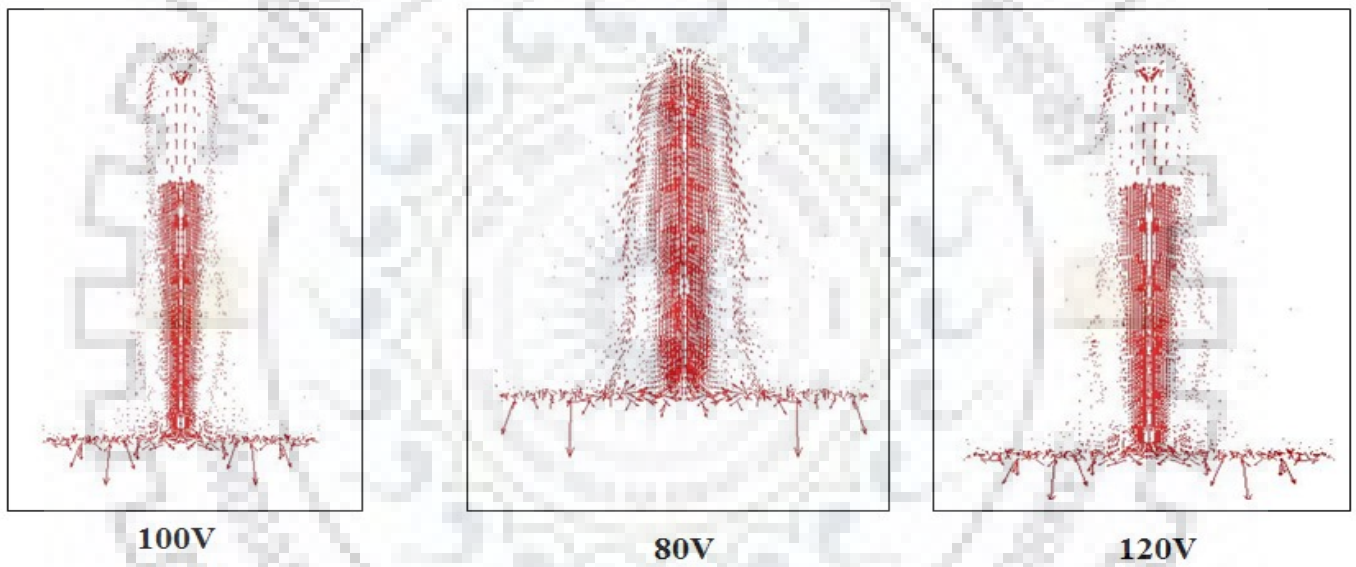
Figure 5.7 Velocity vectors during the collision of the droplet with the solid surface with different actuation potentials.

5.2.2 Variation of Contact Radius

At 0.02 s, droplet is just touching the surface and after that it tries to spread over the surface due to its surface tension (Figure 5.8). Due to electric field electrostatic force are generated. Initially contact radius increases but the inertial force is more than the electrostatic force. After few seconds the repulsive electrostatic force dominates over the surface tension and the kinetic energy of the drop.

Figure 5.8 Variation of contact radius of droplet as a function of time for different actuation
potential; elevation of the drop= 0.00245m.
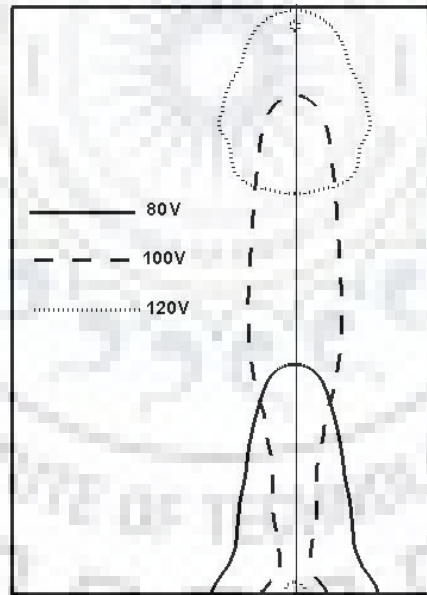
Figure 5.9 Representation of droplet position along the vertical axis for different actuation voltage
at time = 0.03sec

Due to the repulsive electrostatic force the droplet tries to bounce back. From the graph, we
can see that at 80 V droplet is not detached from the surface. Here, due to electrostatic force
droplet tries to retract back but after certain time droplet becomes stable over the surface. As

43

the electric field increases, the electrostatic force increases and tries to bounce back the droplet. So at 100 V due to more electrostatic force droplet is bouncing back from the surface at 0.036 s. At 120V the electrostatic force is much more than the 100 V, so droplet is detached from the surface much earlier than 100 V. Here droplet is detached from 0.03 s. From Figure 5.9 we can see the comparative nature of positions of the droplet when three different voltages are applied. Effect of voltage is clearly identifiable in this figure.

5.2.3 Variation of Contact Line Velocity

Variation on the contact line velocity with respect to time is very important graphical representation to understand the physical behavior of droplet impact on the electrodes. From Figure 5.10 one can see that at 0.02 sec the droplet is touching the surface. Initially, we can see that the contact line velocity increases because the kinetic energy of droplet is more than the electrostatic force. Due to the more kinetic energy the droplet tries to spread over the surface.
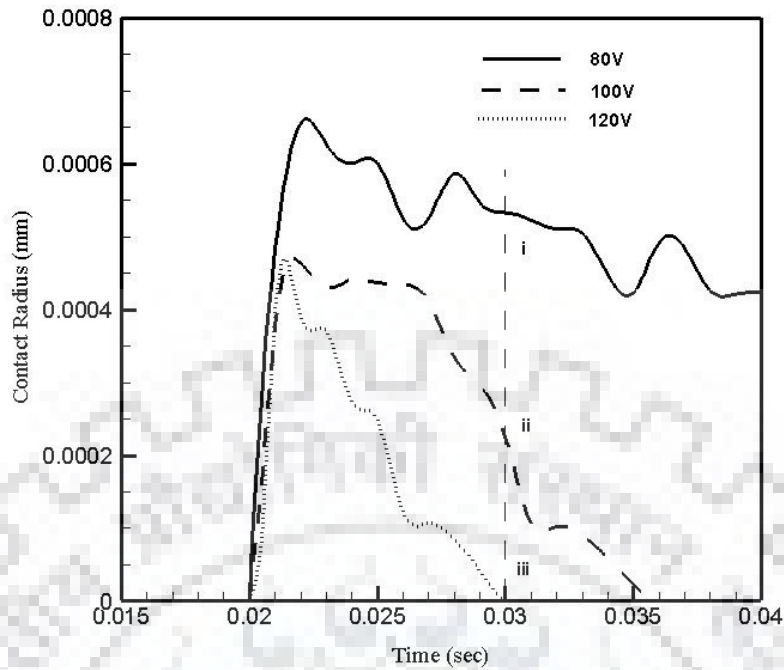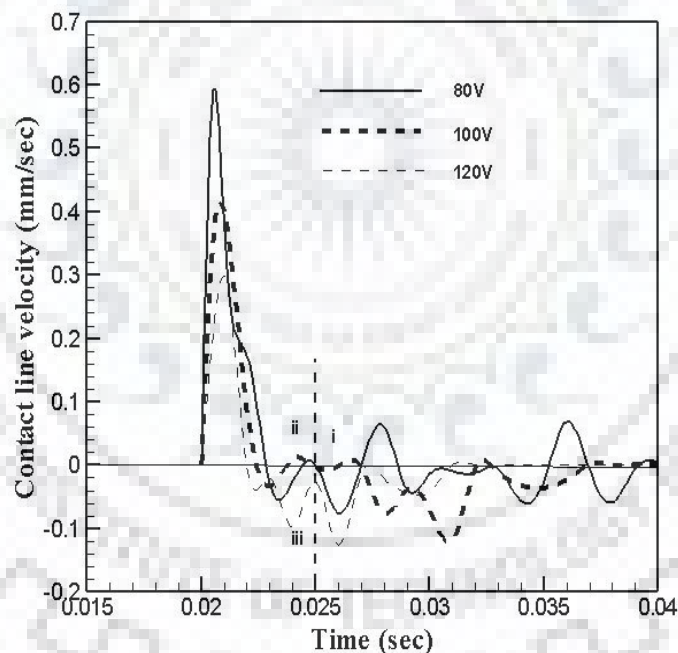

Figure 5.10 Variation of contact line velocity of droplet as a function of time for different actuation potential; elevation of the drop= 0.00245 mm.

For 80V as the electrostatic force is less so contact line spreading velocity is more. As voltage increases from 80 V to 100 V, the repulsive electrostatic force per unit volume increases. So contact line spreading velocity decreases and droplet tries to retract back

towards center. Here the negative velocity shows the retraction tendency of the droplet. For 120 V the repulsive velocity is more rather than 100 and 80V respectively.
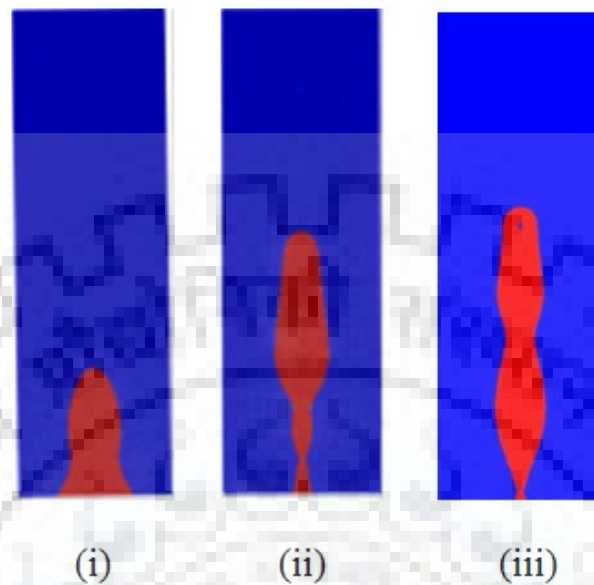
Figure 5.11 Phase contour of the droplet during different actuation voltages at time = 0.025 s, (i) 80 V,(ii) 100 V, (iii)120 V

(a)   (b)   (c)   (d)   (e)   (f)   (g)   (h)
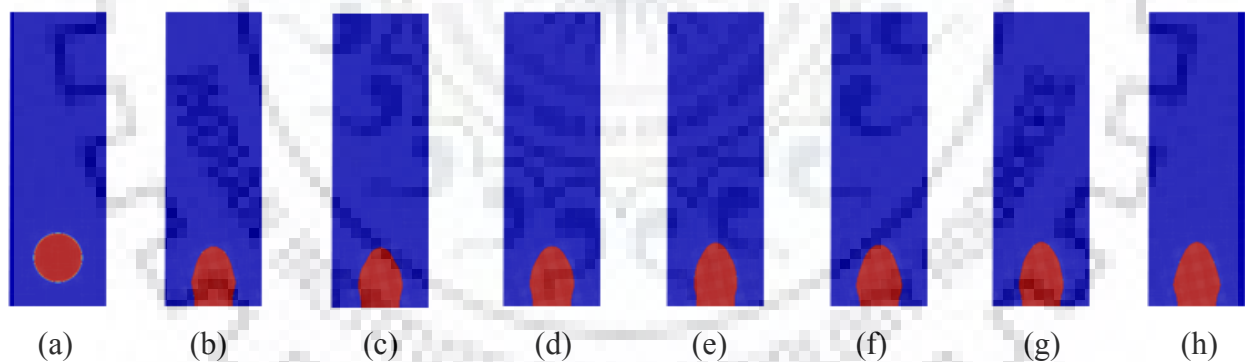
Figure 5.12: Phase contour of the droplet during impact from 1 mm height from base at different time instants. (a) t= 0.0 s, (b) t= 0.0206 s, (c) t= 0.0222 s, (d) t= 0.0247 s, (e) t= 0.0268 s, (f) t= 0.03044 s, (g) t= 0.03277 s, (h) t=0.03776 s

From this study, one can conclude that with increase in voltage keeping all other parameter constant, the contact line spreading velocity decreases but at the same time contact lines retraction velocity increases. So at the higher voltage, droplet tries to jump or bounce back

from the surface. From Figure 5.11 we can also see that phase contour of the droplet during different actuation voltage at time 0.025 s.

5.3 Effect of Impact Height on Drop Impact

Simulations are performed and results are used to compare the droplet contours for three different impact heights, along with electric field applied to the ring electrodes. Figure 5.12-5.14, depicts the phase contours for different drops falling from 1, 1.5 and 3.5 mm heights. It can be observed that droplet bounces back at a faster rate when impact height increases. This can be explained from the increase in extent of inertial force over applied electromotive force for droplet retractions and hence bounce back.

(a)   (b)   (c)   (d)   (e)   (f)   (g)   (h)
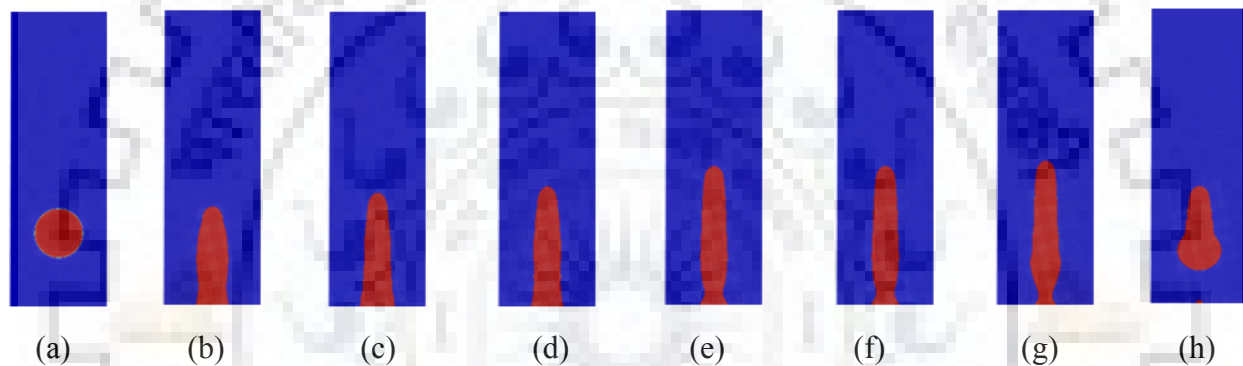
Figure 5.13: Phase contour of the droplet during impact from 1.5 mm height from base at different time instants. (a) t= 0.0 s, (b) t= 0.0206 s, (c) t= 0.0222 s, (d) t= 0.0247 s, (e) t= 0.0268 s, (f) t= 0.03044 s, (g) t= 0.03277 s, (h) t=0.03776 s

(a)   (b)   (c)   (d)   (e)   (f)   (g)   (h)
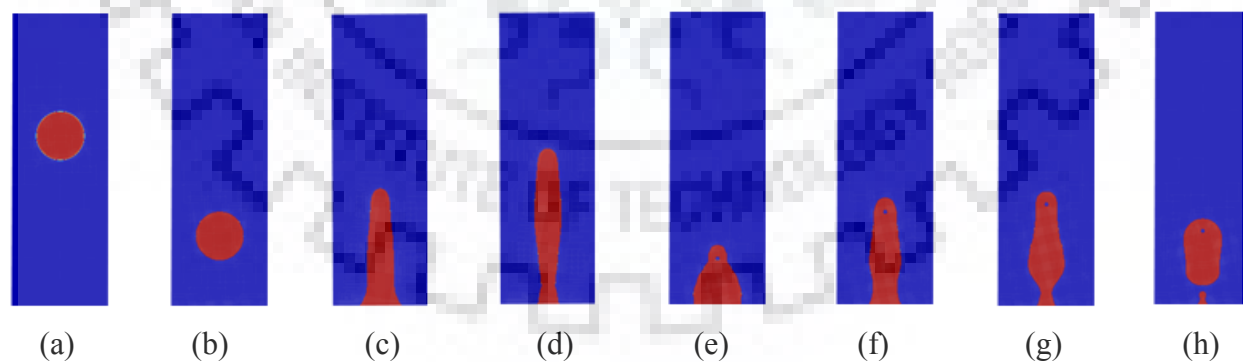
Figure 5.14: Phase contour of the droplet during impact from 3.5 mm height from base at different time instants. (a) t= 0.0 s, (b) t= 0.0206 s, (c) t= 0.0222 s, (d) t= 0.0247 s, (e) t= 0.0268 s, (f) t= 0.03044 s, (g) t= 0.03277 s, (h) t=0.03776 s

During comparison of droplet wettability upon application of different impact heights of droplet, the transition is found in between 1 mm and 1.5mm for 100V.
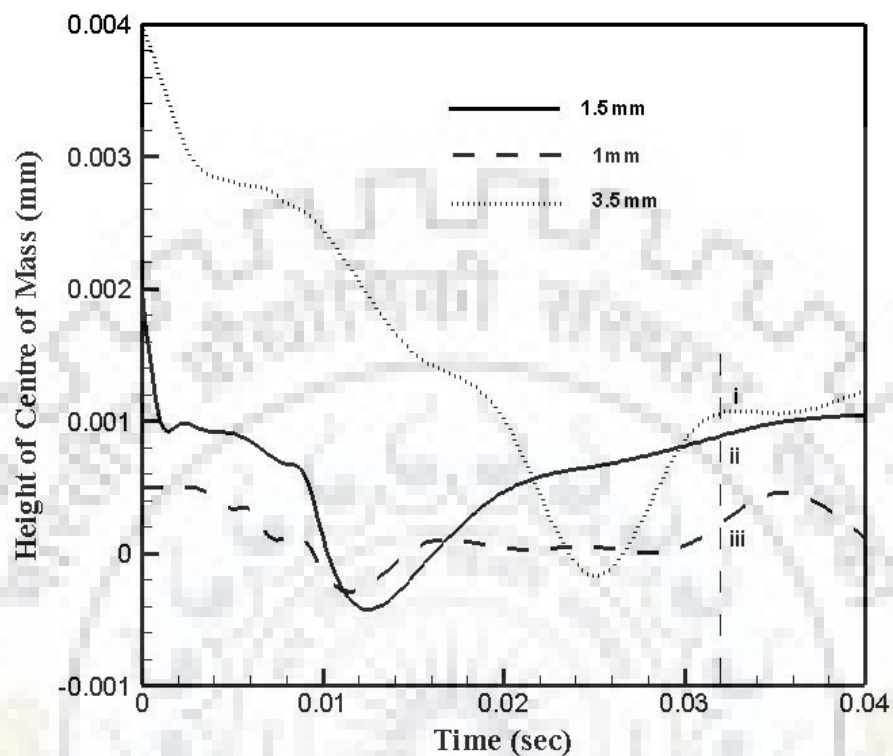

Figure 5.15 Variation of location of the mass center of the droplet as a function of time for different impact height of droplet; at voltage=100V.

5.3.1 Variation of Location of the Mass Center

In this section, analysis of hydrodynamics inside droplets falling from different impact heights is discussed. Figure 5.15 represents the variation of the droplet centre of mass location along the vertical direction with time for different initial heights. The equilibrium contact angle and actuation potential is kept constant at 90° and 100 V, respectively. Droplet, initiated into higher elevation, possesses higher velocity during the downward motion and thus the slope of the curve (during downward motion) is higher than the droplet, started from low height. As the electrostatic force is same for all the three elevations, the inertia of the droplet during impact is the determining factor for the nature of impact dynamics. For droplet with 3.5 mm elevation, the force due inertia is predominant over the electrostatic force. Thus, the spreading front crosses electrostatic force barriers and wetting of the surface occurs. As this phenomenon is more irreversible or deviate more from its

equilibrium so for getting more retraction velocity, droplet tries to come in equilibrium position. Irreversibility will be more for a drop which falls from a large distance (3.5 mm). When the droplet is falling from 1 mm, due to less irreversibility, less retraction velocity is obtained.
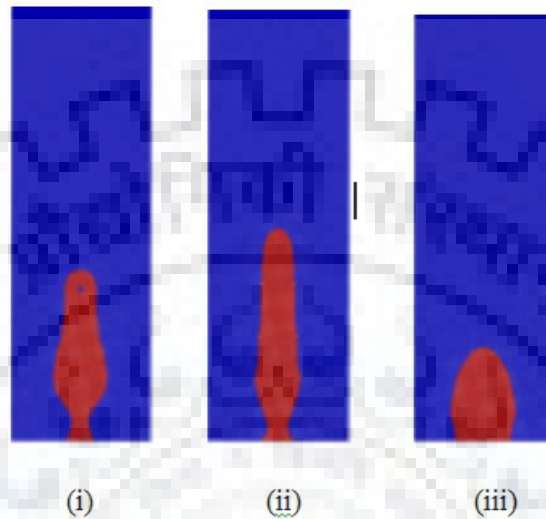
Figure 5.16 Phase contour of the droplet during different impact height at time = 0.032 s, (i) 3.5 mm, (ii) 1.5 mm, (iii) 1 mm

From Figure 5.16 we can also see that phase contour of the droplet during different impact heights at time 0.032 s. When the droplet is stuck from 1 mm height of the electrode, till 0.032 s, droplet is not detached from the surface. But when droplet has been released from 1.5 mm from the surface, droplet tries to bounce back and detach from the surface at the same time. On the other hand when the droplet is freely falling from the surface at 3.5 mm height, droplet bouncing tendencies will be more which can be seen from Figure 5.16.

From Figure 5.17, one can see the velocity vectors inside the droplets to understand the underlying physics. Here, one can compare field velocity vectors for different impact heights of constant actuation potential and contact angles at the same time. When the droplet is retracting back a strong jet is generated through the center which provides potential for bouncing back the droplets. The jet formation is more predominant when the droplet impact height will be more i.e. for 3.5 mm. It lessens gradually for 1.5 and 1 mm height, respectively. For 1 mm impact height the jet formation is not so strong so that it cannot detach from the surface.
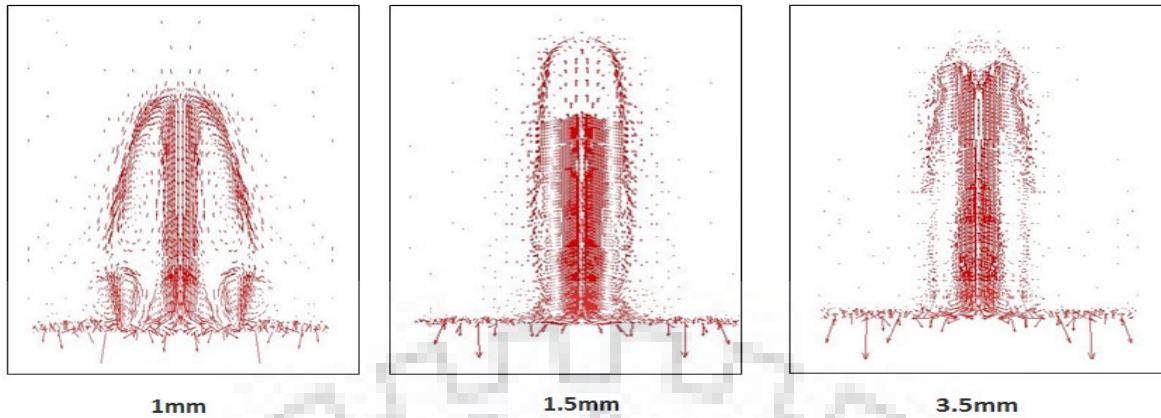
Figure 5.17 Velocity vectors during the collision of the droplet with the solid surface with different impact height.

5.3.2 <u>Variation of Contact Radius</u>

Like the effect of electric potential, efforts are made to observe the spread of contact radius for actuated droplet falling from different heights. It is important to understand the physics behind change in impact behavior. From Figure 5.18, one can see that when the droplet is falling from the lesser height (1 mm) droplet bouncing is not seen. On the other hand, when the droplet is jumping from larger heights the tendency towards droplet jumping is more. As the height is increased keeping all other parameters constant the kinetic energy of droplet is increasing the spreading tendency. But due to actuation, constant electrostatic force repulse back the droplet by stopping spread tendency and droplet retracts back. When the droplet is jumping from more impact heights, the retraction velocity is also more. Hence, contact radii decrease fast during impact from more height. Both velocity of spread and retraction are functions of height before impact. When the height is more bouncing tendencies is also being more because of increasing potential energy.

From Figure 5.19 one can also see that phase contours of the droplet falling from three different impact heights at time 0.032 s. It shows that the droplet sticks with the surface whenever it has fallen from lesser heights i.e. 1 mm. But with increase in impact height, at 1.5 mm droplet reduces its contact radius and elongates at 0.032 s. At 3.5 mm impact height, droplet almost necks down and pinch off from surface. This can be seen from the phase contours diagram.

Figure 5.18 Variation of contact radius of droplet as a function of time for different impact height of droplet; at voltage=100V

(ii)   (iii)   (i)
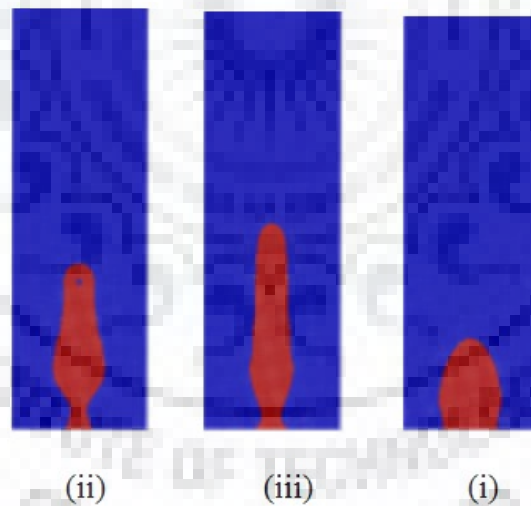
Figure 5.19 Phase contour of the droplet during different impact heights at time = 0.032sec i) 1 mm; ii) 1.5 mm and iii) 3.5 mm

5.3.3 Variation of Contact Line Velocity

There are two types of velocities along the contact line i.e. spreading and retracting. From Figure 5.20 contact line spreading velocity can be found for different simulations having

same contact angle and actuation voltage but different impact height. Contact line velocity shows a peak in velocity during its downfall. This peak can be observed for at a faster rate if it falls from small height. Hence, 1 mm height of impact has the sharpest and fastest peak. On the other hand at 3.5 mm, the peak occurs very late and its amplitude is also not strong. After touching the charged substrate, drop falling from 1.5 mm and 3.5 mm shows negative velocity resembling tendency to rebound. Because the entropy within the droplet for 3.5 mm height will be more so it tries to come back in equilibrium at very faster rate rather than others. So due to more retraction velocity, the droplet tries to bounce back or detach from the surface. At 0.029 s, one can see the position of droplet over the surface. So when the droplet is falling from 1 mm it is in stable position at that particular time, retraction velocity is more when droplet is falling from 3.5 mm.
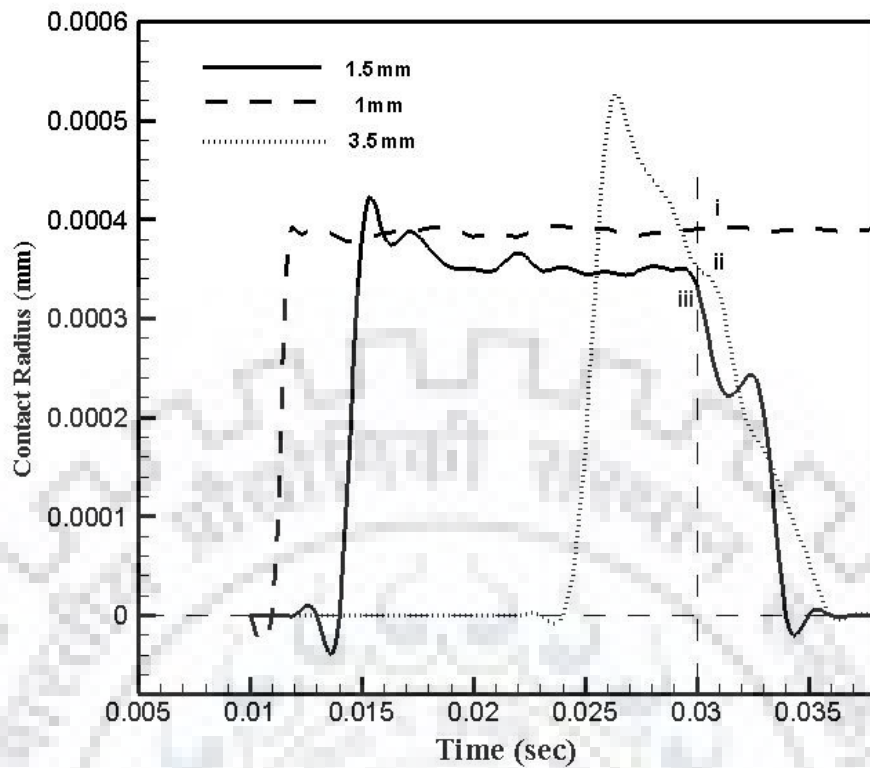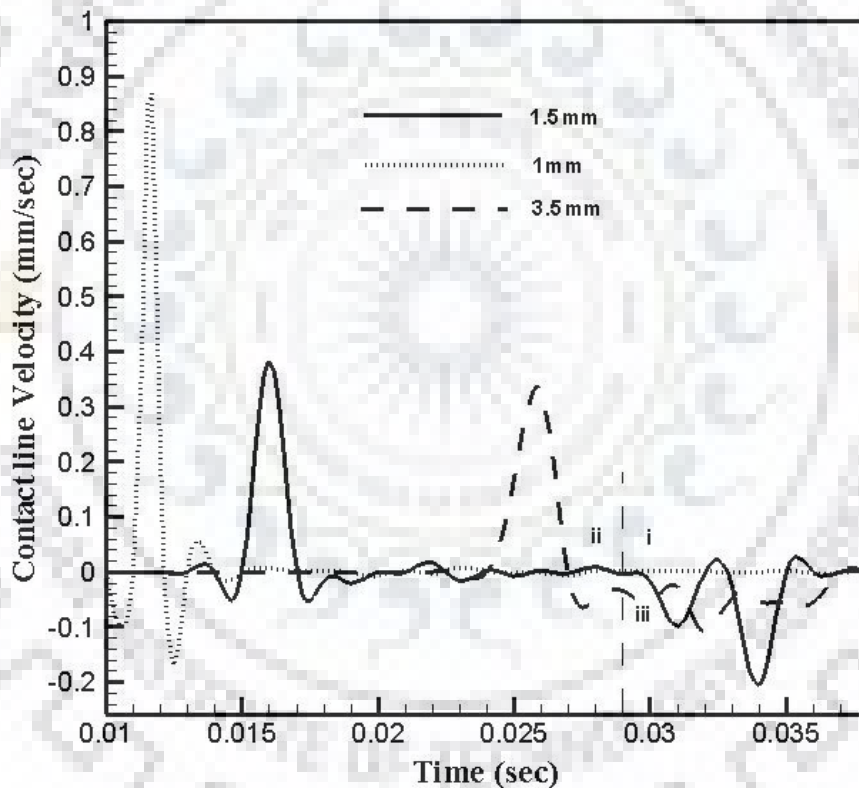

Figure 5.20 Variation of contact line velocity of droplet as a function of time for different impact height of droplet; at voltage=100 V

From Figure 5.21, one can see that the representation of droplet position for different impact heights along the vertical axis for same actuation voltage, at time = 0.03 s. Due to less impact height the droplet is not detached from the surface at 1 mm but at 1.5 mm the

elongation of droplet along the vertical axis is much more and for 3.5 mm the droplet is further elongated and tries to detach from surface.
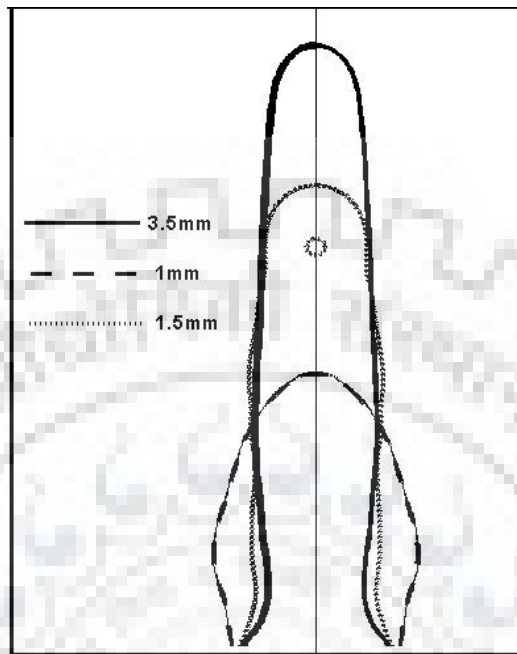
Figure 5.21 Representation of droplet position along the vertical axis for different impact height at time = 0.03 s
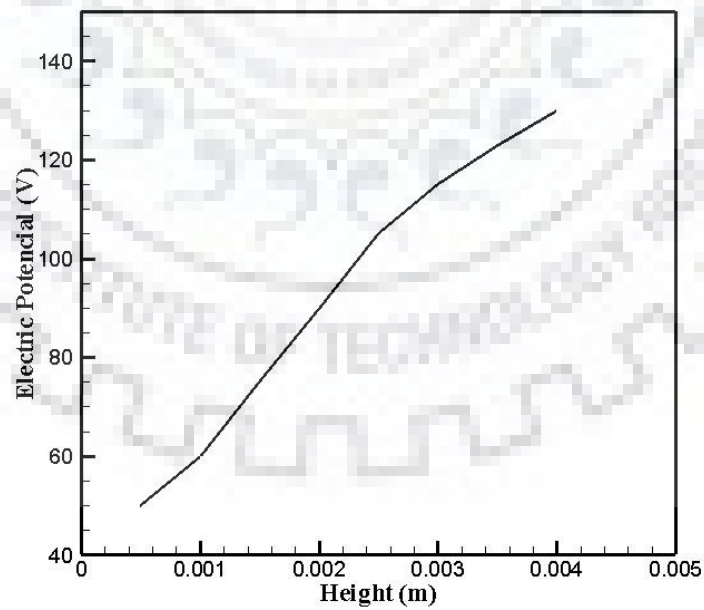
Figure 5.22 Variation of the threshold voltage required for droplet rebound as a function of initial elevation; contact angle 90°.

From the foregoing discussion it is evident that, voltage requirement varies to obtain pseudo super-hydrophobic characteristic for different droplet velocities. Thus, effort has been made to determine the minimum electric potential required for droplet detachment. Figure 5.22 depicts the variation threshold electric potential required for droplet rebound as a function of initial elevation. From the slope of the curve, it can be concluded that the threshold electric potential to obtain the pseudo super-hydrophobic behavior of the substrate is more sensitive at the lower elevations.

| (a) | (b) | (c) | (d) | (e) | (f) | (g) | (h) |
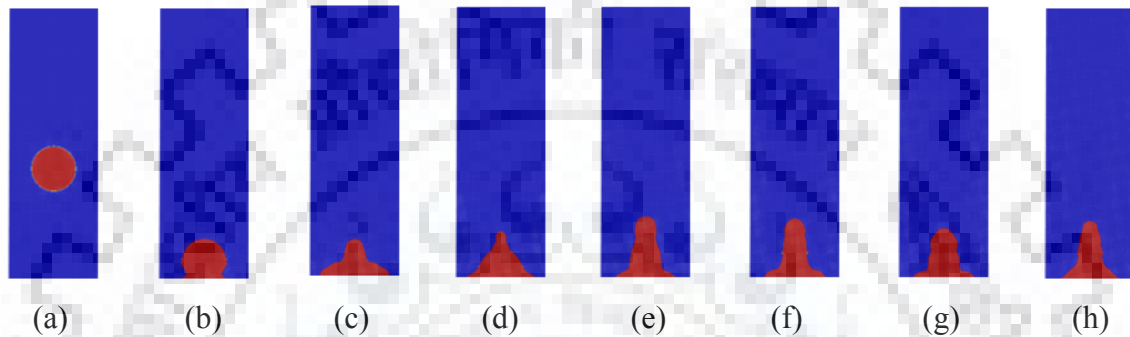
Figure 5.23: Temporal evolution of the phase contour during the impact for 30^0 contact angle. (a) t= 0.0 s, (b) t= 0.0206 s, (c) t= 0.0222 s, (d) t= 0.0247 s, (e) t= 0.0268 s, (f) t= 0.03044 s, (g) t= 0.03277 s, (h) t=0.03776 s; $\phi = 100\,\text{V}$

## 5.4 Effect of Surface Hydrophobicity (Contact Angle) on drop impact

Efforts have also been made to analyze the influence of wetting nature of the surface on the electrostatic manipulation of droplet impact. The wetting nature is characterized by the contact angle made by a liquid-gas interface, with the solid surface. Simulation has been performed by varying the contact angle from 30° to 60°. As representative cases, the temporal evolution of the liquid-gas interface during the impact for the contact angles of 30°, 45° and 60° are shown in Figure 5.23, 5.24 and 5.25 respectively. For the case with 30° contact angle, capillary force of the spreading front dominates over electrostatic constraint. As a consequence it overcomes the electrostatic force and the droplet got attached to the surface upon impact. On the other hand, the electrostatic force is sufficient enough to restrain the contact line motion in the outward direction. This pushes the liquid toward the axis of symmetry and the bouncing occurs. Moreover, due less capillary force in

the case with 60°, the electric force is able to restrict the spreading front earlier. As a consequence, droplet bounces back at a faster rate in this case.

(a)   (b)   (c)   (d)   (e)   (f)   (g)   (h)
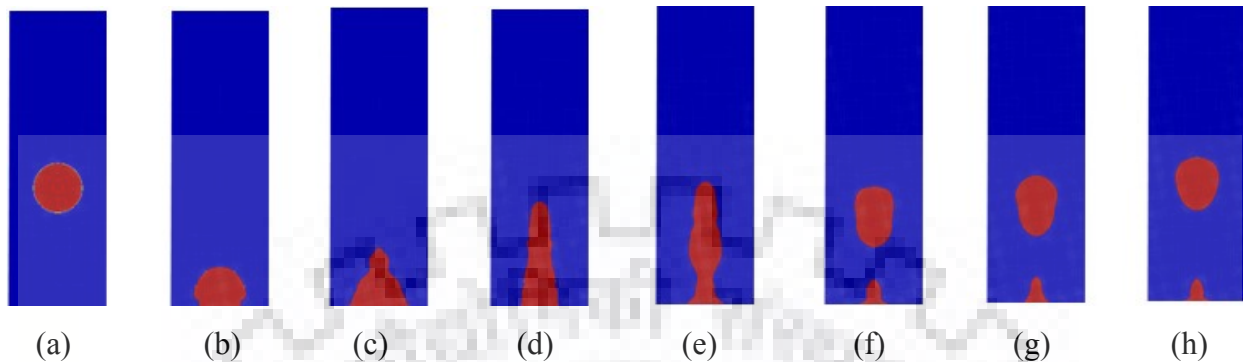
Figure 5.24: Phase contour of the droplet during impact of 45^0 contact angle from base at different time instants. (a) t= 0.0 s, (b) t= 0.0206 s, (c) t= 0.0222 s, (d) t= 0.0247 s, (e) t= 0.0268 s, (f) t= 0.03044 s, (g) t= 0.03277 s, (h) t=0.03776 s

(a)   (b)   (c)   (d)   (e)   (f)   (g)   (h)
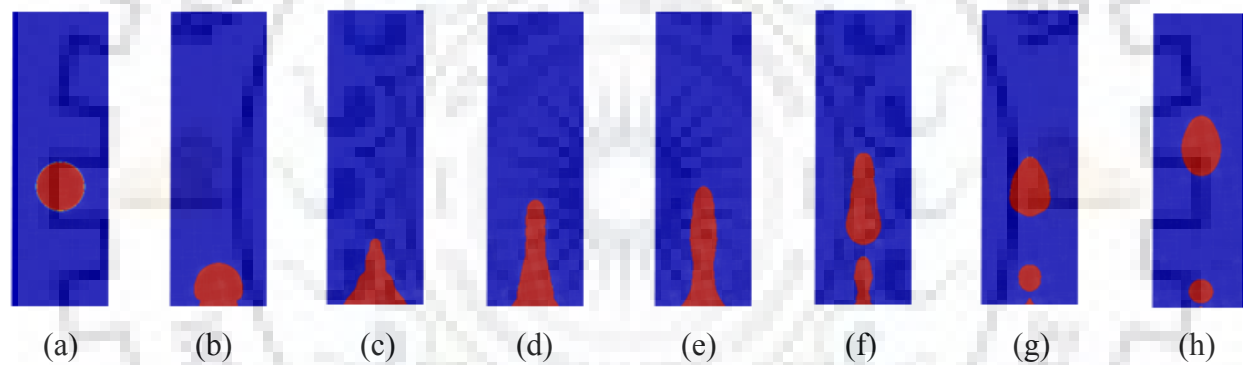
Figure 5.25: Phase contour of the droplet during impact of 60^0 contact angle from base at different time instants. (a) t= 0.0 s, (b) t= 0.0206 s, (c) t= 0.0222 s, (d) t= 0.0247 s, (e) t= 0.0268 s, (f) t= 0.03044 s, (g) t= 0.03277 s, (h) t=0.03776 s

5.4.1 Variation of Location of the Mass Center

To analyze the phenomenon observed in the above section quantitatively, the vertical location of the droplet mass center is tracked with time. Figure 5.26 depicts the variation of the height of the droplet mass center as a function of time. In all the cases the elevation and the actuation potential is kept constants at 0.00195 m and 100 V respectively. For a relatively more hydrophilic surface (contact angle = 30°), as the droplet got stuck to the surface, the height of the mass center does not vary much after the impact. Whereas, for the impact on the surfaces with 45° and 60° contact angle, the curves changed its slope as the

droplets starts its upward journey after the collision. Relatively larger dominance of the electrostatic force for the case with 60° contact angle causes higher upward velocity of the droplet and thus steeper slope in the curve. The relatively higher degree of electrostatic restriction to the outward flow pushes more liquid toward the axis of symmetry causing a central jet with a higher strength. This in turn elongates the droplet along the direction of motion. The shape of the droplets after 0.03 s shown in figure 5.27. This elongation of the droplets also augments the upward displacement of mass center with time.

Figure 5.26 Variation of the droplet mass center location as a function of time for different contact angle; at voltage 100 V

(i)   (ii)   (iii)
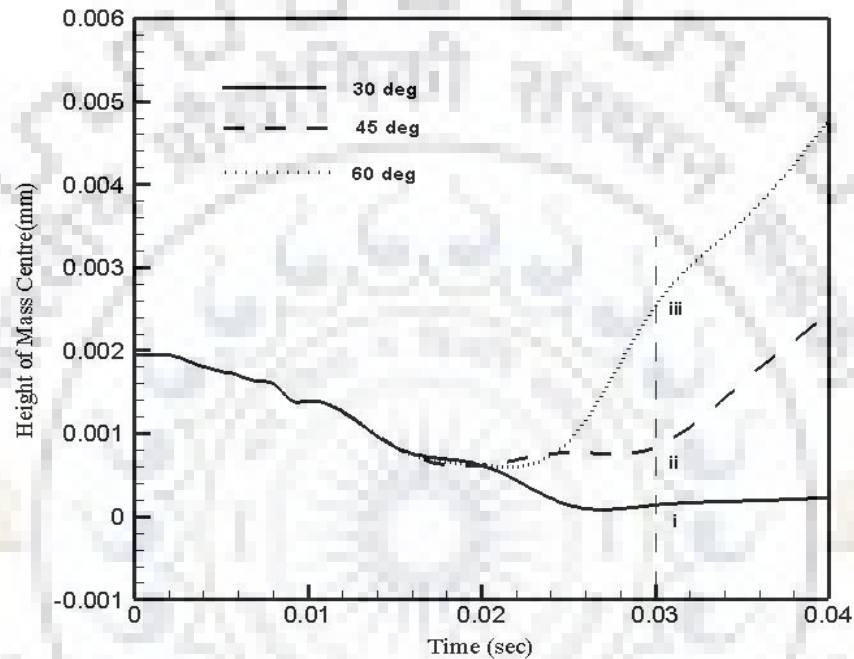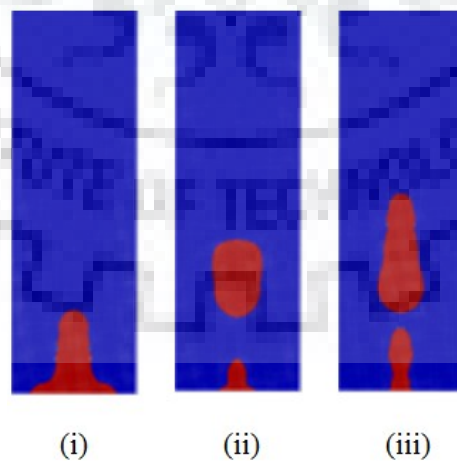
Figure 5.27 Phase contour of the droplet during the impact for different contact angle case, at time = 0.03 s; (i) 30°, (ii) 45°, (iii) 60°

To dig down further, velocity vectors inside the flow domain is analyzed. Figure 5.28, shows the velocity vectors inside the flow domain at 0.03 s for different contact angles. For the case of impact on a surface with 60° substrate contact angle, the strong stream inside the core region elongates the droplet. A neck is formed at the lower portion of the droplet due to capillary instability. Eventually, the droplet breaks in two parts. The large droplet created from the upper portion of the bulk continues its upward motion showing upward velocity vectors. Surface tension become dominant in the portion of the droplet attached to the surface due its smaller size. The capillary force arises from the deformation tries to bring the liquid mass to a hemispherical shape. This, causes velocity vectors to at downward direction. On the other hand, for the case with 30° angle, the inertia of the vertical is not enough to move the interface upward. Thus, after a certain elongation it possesses downward velocity as evident from the velocity vectors (Figure 5.28 (c)).

60 deg   45deg   30deg

(a)   (b)   (c)
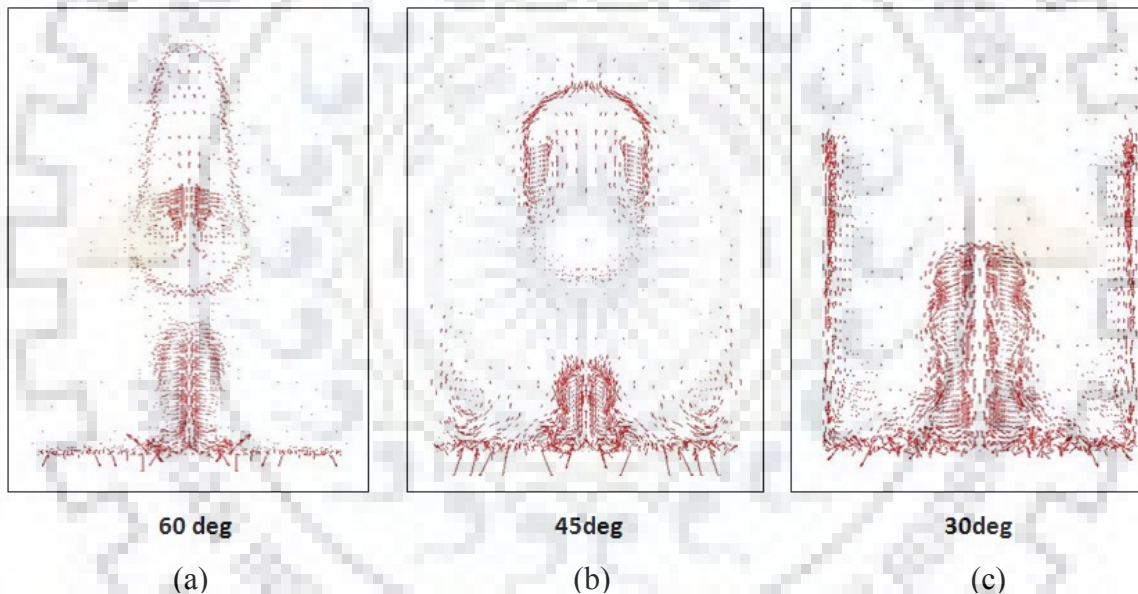
Figure 5.28 Velocity vectors inside the flow domain at 0.03 s during the impact for different contact angle situations.

5.4.2 Variation of Contact Radius

Figure 5.29 elucidates the variation of spreading radius as a function of time. It can be observed from the figure that, up to a certain time period the contact radius increases at a same rate. This, signifies the fact that, the spreading does not depend much on the electric field and the hydrodynamics is mainly governed by the capillary force it this stage. The

influence of electric field is evident beyond this time period. Due to the high capillary force, the case with 30° contact angle achieved maximum spreading radius.
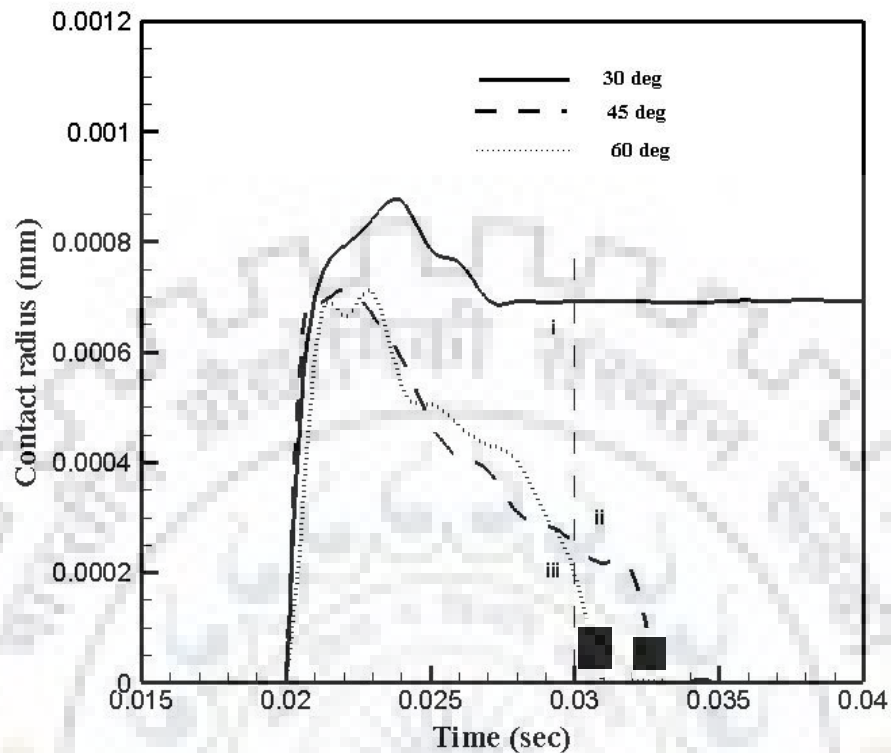
Figure 5.29 Variation of contact radius of droplets as a function of time for different contact angle; at voltage 100 V.

Moreover, it shows an approximately constant spreading radius after showing some initial recoiling. On the other hand, the cases with the contact angle of 45° and 60°, the droplet recoils back to a very small contact radius (due to the formation of the daughter droplet the contact radius never become zero). Here, it has to be mentioned that, for these cases, the contact radius is measured till the pinch off of the daughter droplets. Initially, the rate of recoiling is same for both the cases. However, due to the dominance of the electrostatic force, the droplet with 60° contact angle recoils faster at the latter stages.

CHAPTER 6

CONCLUSION

6.1 <u>CONCLUSION</u>

An electro-hydrodynamic model is considered to investigate the dynamics of droplet impact with a solid surface under the influence of external electric field. The study reveals a superhydrophobic nature of the surface under the electrostatic actuation (at concentric ring shaped regions). The electric field a vector inside the domain reflect that, there is a resistance force to the spreading of contact line exists at the half span of the electrode due to the change of direction of the same. The interplay between the inertia and electrostatic force is analyzed for different parameters like electric potential, initial elevation and contact angle. Result shows that, at a low voltage the propagation of the wetting front over a hydrophobic surface can overcome the electrostatic resistance. The study also reveals that, the contact radiuses of droplet as well as contact line velocity variation with respect to time are also studied. The result of the present investigation can be utilized to design tunable hydrophobic surfaces for the applications in various microfluidic operations.

Present research work deals with droplet dynamics with the application of electric field. My research work revealed the following observations:

6.2 Impact dynamics of droplet:

➤ The hydrophilic surface can be transformed into hydrophobic surface using electrostatic actuation.

➤ When a droplet falls on a hydrophilic surface, it sticks to because the electrostatic forces are not enough to pin down the contact line of spreading in the outward direction.

➤ As electric field is applied to certain limit, the droplet bounces back in upward direction i.e. electrostatic forces over comes the contact line of spreading. This strength is referred as critical value.

➤ The critical strength of electric field required to bounce back the droplet in upward direction increases with increase with initial height of droplet due to inertia of the droplet.

➤ Lesser contact angle between the droplet and the surface favors the bouncing of droplet i.e. critical strength of electric field required to bounce back the droplet in upward direction decreases in decrease in contact angle.

➤ From our simulation we can see that as the voltage is increasing the droplet bouncing tendencies will be more. So the bounce back droplet mass center height is more for higher voltage.

➢ As for increasing voltage the electrostatic repulsive force is more w.r.t the inertia force so the droplet spreading over the electrode will be less and well as contact radius will be less for higher voltage.

➢ As the voltage is increasing keeping all other parameter constant the contact line spreading velocity decreases but at the same time contact lines retraction velocity is increases.

➢ From these simulations we can see that as the impact height is increasing the droplet bouncing tendencies will be more. So the bounce back droplet mass center height is more for higher impact height.

➢ When the height is more bouncing tendencies is also being more because when height is increasing potential energy is increasing. so contact line spreading will be less for more impact height.

➢ For more impact height contact line velocity will be less and retraction velocity will be more.

➢ From our simulation we can also see that as the contact angle is increasing the droplet bouncing tendencies will be more. So the bounce back droplet mass center height is more for higher contact angle.

➢ Retraction velocity will be more for hydrophobic nature so the droplet bouncing tendencies will also be more for higher contact angle.

6.3 Future Scope:

➢ Droplet adhesion on engineering hydrophobic surface for better heat transfers can be tried with application of electric field. The idea will be important to soft matter, chip cooling applications.

➢ Creation of daughter droplet using electric field will be another direction which will be of interest in multitudes of microfluidic applications. Production of micron size droplets are very difficult using body force. Application of electric field may be tried in this direction.

➢ Application of the negative voltage over the electrode may transform hydrophobic surface to hydrophilic surface.

REFERENCES

[1] Tsai, P., Hendrix, M.H., Dijkstra, R.R., Shui, L. and Lohse, D., 2011. Microscopic structure influencing macroscopic splash at high Weber number. Soft Matter, 7(24), pp.11325-11333.

[2] Bhushan, B., Jung, Y.C. and Koch, K., 2009. Micro-, nano-and hierarchical structures for superhydrophobicity, self-cleaning and low adhesion. Philosophical Transactions of the Royal Society of London A: Mathematical, Physical and Engineering Sciences, 367(1894), pp.1631-1672.

[3] Lippmann, G., 1873. Beziehungen zwischen den Capillaren und elektrischen Erscheinungen. Annalen der Physik, 225(8), pp.546-561.

[4] Berge, B., 1993. Electro capillarity and wetting of insulator films by water. Competes Rendus De L Academie Des Sciences Serie Ii, 317(2), pp.157-163.

[5] Kuiper, S. and Hendriks, B.H.W., 2004. Variable-focus liquid lens for miniature cameras. Applied physics letters, 85(7), pp.1128-1130.

[6] Yi, Z., Shui, L., Wang, L., Jin, M., Hayes, R.A. and Zhou, G., 2015. A novel driver for active matrix electrowetting displays. Displays, 37, pp.86-93.

[7] Cho, S.K., Moon, H. and Kim, C.J., 2003. Creating, transporting, cutting, and merging liquid droplets by electrowetting-based actuation for digital microfluidic circuits. Journal of microelectromechanical systems, 12(1), pp.70-80.

[8] Cho, S.K., Fan, S.K., Moon, H. and Kim, C.J., 2002, January. Towards digital microfluidic circuits: creating, transporting, cutting and merging liquid droplets by electrowetting-based actuation. In Micro Electro Mechanical Systems, 2002. The Fifteenth IEEE International Conference on (pp. 32-35). IEEE. [9] John S. Eow, Mojtaba Ghadiri , Chemical Engineering and Processing,2003, 259-274.

[10] Lee, S.J., Hong, J., Kang, K.H., Kang, I.S. and Lee, S.J., 2014. Electrowetting-induced droplet detachment from hydrophobic surfaces. Langmuir, 30(7), pp.1805-1811.

[11] Aminfar, H. and Mohammadpourfard, M., 2012. Droplets merging and stabilization by electrowetting: Lattice Boltzmann study. Journal of Adhesion Science and Technology, 26(12-17), pp.1853-1871.

[12] Arzpeyma, A., Bhaseen, S., Dolatabadi, A. and Wood-Adams, P., 2008. A coupled electro-hydrodynamic numerical modeling of droplet actuation by electrowetting. Colloids and Surfaces A: Physicochemical and Engineering Aspects,323(1), pp.28-35.

[13] Datta, S., Das, A.K. and Das, P.K., 2015. Uphill movement of sessile droplets by electrostatic actuation. Langmuir, 31(37), pp.10190-10197.

[14] Banerjee, A.N., Qian, S. and Joo, S.W., 2011. High-speed droplet actuation on single-plate electrode arrays. Journal of colloid and interface science, 362(2), pp.567-574.

[15] Datta, S., Das, A.K. and Das, P.K., 2016. Unravelling Electrostatic Actuation on Inclined and Humped Surfaces: Effect of Substrate Contact Angle. Industrial & Engineering Chemistry Research, 55(14), pp.3949-3959.

[16] Lee, M.W., Latthe, S.S., Yarin, A.L. and Yoon, S.S., 2013. Dynamic electrowetting-on-dielectric (DEWOD) on unstretched and stretched teflon. Langmuir, 29(25), pp.7758-7767.

[17] Daub, C.D., Bratko, D., Leung, K. and Luzar, A., 2007. Electrowetting at the nanoscale. The Journal of Physical Chemistry C, 111(2), pp.505-509.

[18] Ghazian, O., Adamiak, K. and Castle, G.S.P., 2013. Electric-field-induced oscillations of water droplets deposited on insulating surfaces. Journal of Electrostatics, 71(3), pp.489-495.

[19] Kuo et al. Droplet Actuation by Electrowetting-on-Dielectric (EWOD): A Review, J. Adhes. Sci. Technol., 26, pp. 1747-1771, 2012.

[20] Wang, Z., Lopez, C., Hirsa, A. and Koratkar, N., 2007. Impact dynamics and rebound of water droplets on superhydrophobic carbon nanotube arrays. Applied physics letters, 91(2), p.023105.

[21] Vallet, M., Vallade, M. and Berge, B., 1999. Limiting phenomena for the spreading of water on polymer films by electrowetting. The European Physical Journal B-Condensed Matter and Complex Systems, 11(4), pp.583-591.

[22] Bahadur, V. and Garimella, S.V., 2007. Electrowetting-based control of static droplet states on rough surfaces. Langmuir, 23(9), pp.4918-4924.

[23] Song, F.H., Li, B.Q. and Liu, C., 2014. Molecular dynamics simulation of the electrically induced spreading of an ionically conducting water droplet. Langmuir, 30(9), pp.2394-2400.

[24] Yuan, Q. and Zhao, Y.P., 2010. Precursor film in dynamic wetting, electrowetting, and electro-elasto-capillarity. Physical Review Letters, 104(24), p.246101.

[25] Popinet, S., 2003. Gerris: a tree-based adaptive solver for the incompressible Euler equations in complex geometries. Journal of Computational Physics, 190(2), pp.572-600.

[26] Popinet, S., 2009. An accurate adaptive solver for surface-tension-driven interfacial flows. Journal of Computational Physics, 228(16), pp.5838-5866.

[27] López-Herrera, J.M., Popinet, S. and Herrada, M.A., 2011. A charge-conservative approach for simulating electrohydrodynamic two-phase flows using volume-of-fluid. Journal of Computational Physics, 230(5), pp.1939-1955.

[28] Khokhlov, A.M., 1998. Fully threaded tree algorithms for adaptive refinement fluid dynamics simulations. Journal of Computational Physics, 143(2), pp.519-543.

ACHIEVEMENT FROM STUDY

Publication in International Journal:

[1] Pal, S., Ansari M., Datta, S., Das A. K., Das, P. K., 2017. Control of Drop Impact and Proposal of Pseudosuperhydrophobicity Using Electrostatics. Industrial and Engineering Chemistry Research, 56, pp. 11312-11319. **(Impact Factor: 2.843)**

Publication in Conference

[1] Pal, S., Datta, S., Das A. K., Das, P. K., Influence of electric field on the hydrodynamics of droplet impact on a solid surface. IHMTC – 2017, Hyderabad, India, 27-30, December 2017, Paper ID: 13-0961.

Appendix A

A.1. Gerris script for the simulation of drop impact with electric field:

```
GModule electrohydro
6 5 GfsElectroHydroAxi GfsBox GfsGEdge {} {
    Global {
    #define R0 0.0005
    #define R 6250000000000
    #define Q 80.225
    #define Ef1 10
    #define Cmu 0.10
    #define F1 1
    #define F2 0
    #define theta 30.
    }
    Time { end = 1}
    VariableTracer Rhoe
    VariableTracerVOFHeight T
    VariableCurvature K T
    SourceTension T 0.072 K
    SourceViscosity {} T*0.00089 + 0.0000181*(1. - T)
    Source {} U -9.81
    Source {} V 0.0

    PhysicalParams { L = 0.001 alpha=1./(T*1000.+(1.-T)*1.1644)  }
    InitFraction T (R0*R0 - ((0.00195-x)*(0.00195-x) + (0.0+y)*(0.0+y)))

    AdaptGradient { istep = 1 } { cmax = 1e-4   maxlevel = 9 } T
    AdaptVorticity { istep = 1 } { maxlevel = (x < 0.0015 ? 9 : 5) cmax = 1e-2 }
    AdaptFunction { istep = 1 } { minlevel = 0 maxlevel = 5 } (T >0 && T < 1)

    SourceElectric
    SourceDiffusionExplicit Rhoe ((1. - T)*(8.0e-15)+ 5.5e-6*T) Phi
```

```
OutputDropletSums { istep = 100 } vol_100 { v = T*dV } T
OutputDropletSums { istep = 100 } volv_100 { v = U*T*dV } T
OutputDropletSums { istep = 100 } volx_100 { v = x*T*dV } T
OutputSimulation { istep = 1 } stdout
OutputTime { istep = 10 } stderr
OutputBalance { istep = 10 } stderr
OutputProjectionStats { istep = 10 } stderr
OutputDiffusionStats { istep = 10 } stderr
OutputScalarSum { istep = 10 } rhoe { v = Rhoe }


GModule gfsview
OutputView {start = 0 istep = 100} {ppm2mpeg -s 1366x768 > view1.mp4 } {
        format = PPM width =1366 height =768     } tr1.gfv
OutputSimulation { istep = 1 } stdout
OutputSimulation { start = end } b.gfs
OutputSimulation { start = 0 istep = 1000 } %g.dat { variables = U,V,T,P,Phi
                                                format = Tecplot }
 EventScript { start = 0 istep = 1000 } { echo "Save t-$GfsTime.eps { format = EPS }" }
 } {
 # Electric parameters
 perm = (710e-12*T + (1. - T)*8.85e-12)
 charge = Rhoe
 ElectricProjectionParams { tolerance = 1e-8 }
 }
 #1
 GfsBox {
 left = Boundary {
 BcDirichlet Phi {if(y>=0.00 && y<0.0001)
            return  80.0;
            else if(y>=0.0002 && y<0.0003)
            return 80.0;
            else if(y>=0.0004 && y<0.0005)
            return 80.0;
            else if(y>=0.0006 && y<0.0007)
```

```
                return 80.0;
                else if(y>=0.0008 && y<0.0009)
                return 80.0;
                else
                return 0.0;
                }
 BcDirichlet U 0.0
 BcDirichlet V 0.0
 BcAngle T 90
 }

bottom = Boundary

top = Boundary{    BcDirichlet Phi 0.0   }
}
#2
GfsBox {
bottom = Boundary

top = Boundary{   BcDirichlet Phi 0.0    }
}
#3
GfsBox {

bottom = Boundary
top = Boundary{    BcDirichlet Phi 0.0     }
}
#4
GfsBox {
bottom = Boundary
top = Boundary{ BcDirichlet Phi 0.0 }
}
#5
GfsBox { bottom = Boundary
top = Boundary{BcDirichlet Phi 0.0  }
}
```

```
#6
GfsBox {
right = Boundary { }

bottom = Boundary
top = Boundary{ BcDirichlet Phi 0.0    }
}

1 2 right
2 3 right
3 4 right
4 5 right
5 6 right
```

A.2. Gfsview script for visualization:

```
# GfsView 2D
View {
  tx = -0.568437 ty = -2.50323
  sx = 1 sy = 1 sz = 1
  q0 = 0 q1 = 0 q2 = -0.706302 q3 = 0.70791
  fov = 30.3373
  r = 0.3 g = 0.4 b = 0.6
  res = 1
  lc = 0.001
  reactivity = 0.1
}
Linear {
  r = 1 g = 1 b = 1
  shading = Constant
  maxlevel = -1
  font_size = 1
  raster_font = 1
  line_width = 1
} {
  n.x = 0 n.y = 0 n.z = 1
  pos = 0
} T {
  amin = 1
  amax = 1
  cmap = Jet
} 0 {
  reversed = 0
```

```
    use_scalar = 1
}
Symmetry {
  r = 0 g = 0 b = 0
  shading = Constant
  maxlevel = -1
  font_size = 1
  raster_font = 1
  line_width = 1
} {
  n.x = 0 n.y = 1 n.z = 0
  pos = 0
}
```